LUND UNIVERSITY

Amyloid beta aggregation kinetics

The role of intrinsic and extrinsic factors.

Yang, Xiaoting

2016

Link to publication

Citation for published version (APA):
Yang, X. (2016). *Amyloid beta aggregation kinetics: The role of intrinsic and extrinsic factors.* [Doctoral Thesis (compilation), Biochemistry and Structural Biology]. Lund University, Faculty of Science, Department of Biochemistry and Structural Biology.

Total number of authors:
1

General rights
Unless other specific re-use rights are stated the following general rights apply:
Copyright and moral rights for the publications made accessible in the public portal are retained by the authors and/or other copyright owners and it is a condition of accessing publications that users recognise and abide by the legal requirements associated with these rights.
• Users may download and print one copy of any publication from the public portal for the purpose of private study or research.
• You may not further distribute the material or use it for any profit-making activity or commercial gain
• You may freely distribute the URL identifying the publication in the public portal

Read more about Creative commons licenses: https://creativecommons.org/licenses/

Take down policy
If you believe that this document breaches copyright please contact us providing details, and we will remove access to the work immediately and investigate your claim.

LUND UNIVERSITY

PO Box 117
221 00 Lund
+46 46-222 00 00

Amyloid β aggregation kinetics

The role of intrinsic and extrinsic factors

XIAOTING YANG | BIOCHEMISTRY AND STRUCTURAL BIOLOGY | LUND UNIVERSITY

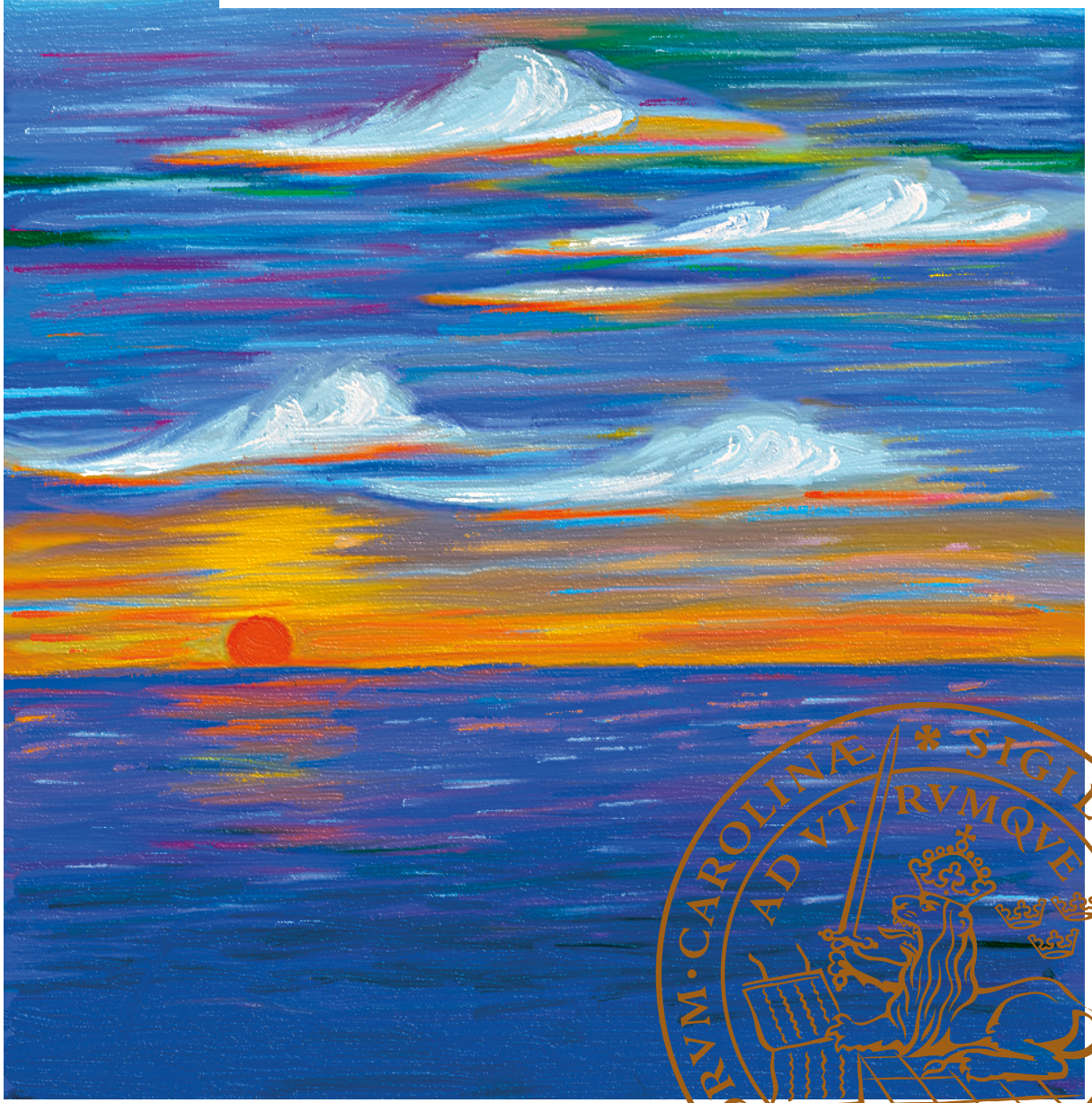

Amyloid β aggregation kinetics
The role of intrinsic and extrinsic factors

by Xiaoting Yang

LUND
UNIVERSITY

Doctoral Thesis
Supervisor: Prof. Sara Snogerup Linse
Cosupervisor: Asso. Prof. Tommy Cedervall
Faculty opponent: Prof. Natàlia Carulla

by due permission of the Faculty of Science of Lund University, Sweden.
To be defended on the 17th of June 2016 at 9.15 in Hall B, Kemicentrum.

Organization
LUND UNIVERSITY

Department of Biochemistry and Structural Biology
PO Box 124
SE–221 00 LUND
Sweden

Author(s)
Xiaoting Yang

Document name
DOCTORAL DISSERTATION

Date of disputation
2016-06-17

Sponsoring organization

Title and subtitle
Amyloid β aggregation kinetics: The role of intrinsic and extrinsic factors

Abstract

Cerebral senile plaque is one of the main pathologies of Alzheimer's disease (AD). The amyloid cascade hypothesis suggests that the aggregation of amyloid β (Aβ) peptide is involved in the pathogenesis of AD, which is supported by the fact that Aβ overexpression or production of more aggregation-prone variants lead to early-onset dementia. In this work, we mainly studied the *in vitro* Aβ aggregation kinetics, to investigate the mechanistic shift as a result of intrinsic factors and extrinsic factors. We employ a fluorescence probe Thioflavin T (ThT) to follow the aggregation kinetics. The aggregation half-time is then extracted and plotted against monomer concentration. By fitting the curve with a power function, a scaling exponent is extracted and reflects the aggregation monomer dependence. The ThT data can be globally fitted using master equations to determine the dominant aggregation reaction step at the microscopic level. Circular dichroism spectroscopy and cryogenic transmission electron microscopy are used to study the fibril structure transition and morphology. Surface plasmon resonance and mass spectrometry provide information of molecular interaction and the latter one is also used to identify peptide segments of the soluble and insoluble Aβ species. Our results show a two-step saturated secondary nucleation dominated mechanism in several cases: Aβ mutants E22K, E22Q, E22G, D23N and A2V, which link to an early-onset of AD, Aβ40 aggregation at high monomer concentration (> 30 μM, pH 7.4), and Aβ42 aggregation at high ionic strength (> 92 mM) and at pH 7.4. The mechanistic shift in these cases is mainly attributed to a reduced repulsion between monomers and other aggregating species due to decreased absolute charges from point mutation or pH shifting to a value close to the isoelectric point, or due to increased ionic strength by adding salt. This effect is combined with additional hydrophobic effect or other side chain properties in some cases to reach a more enhanced secondary nucleation. The secondary nucleation that produces enormous amount of toxic oligomers is found to be severely inhibited by a chaperone protein, Brichos, through specifically binding to the fibril surface and blocking the catalytic cycle. In our co-aggregation work, the most abundant Aβ variants, Aβ40 and Aβ42 that differ in length at C-terminus, do not co-aggregate and do not form mixed fibrils. The result implies that Aβ40 and Aβ42 interact exclusively at primary nucleation level and Aβ aggregation is a highly selective process that tolerates a low level of sequence mismatch in C-terminus.

Key words
Alzheimer's disease, Aβ, aggregation, kinetics, secondary nucleation

Classification system and/or index terms (if any)

Supplementary bibliographical information

Language
English

ISSN and key title

ISBN
978-91-7422-465-8

Recipient's notes

Number of pages
192

Price

Security classification

I, the undersigned, being the copyright owner of the abstract of the above-mentioned dissertation, hereby grant to all reference sources the permission to publish and disseminate the abstract of the above-mentioned dissertation.

Signature Xiaoting Yang Date 2016-05-17

DOKUMENTDATABLAD enl SIS 61 41 21

Amyloid β aggregation kinetics
The role of intrinsic and extrinsic factors

by Xiaoting Yang

LUND
UNIVERSITY

Cover illustration front: All is well.

Funding information:

The thesis work was financially supported by China Scholarship Counsil and European Research Counsil.

© Xiaoting Yang 2016

Faculty of Science, Department of Biochemistry and Structural Biology

ISBN: 978-91-7422-465-8

Printed in Sweden by Media-Tryck, Lund University, Lund 2016

Dedicated to my families
Yuzhen – Wangyun – Zhidong

Contents

Popular science summary . . . iii
论文简介 . . . v
Acknowledgements . . . vii
List of papers . . . xi
My contribution to the papers . . . xii
List of abbreviations . . . xiii

Introduction **1**
Alzheimer's disease and amyloid β peptide . . . 1
Pathology of Alzheimer's disease . . . 1
Amyloid cascade hypothesis . . . 2
Amyloid precursor protein and amyloid β peptide . . . 3
Early-onset familial Alzheimer's disease . . . 4
Aβ aggregation kinetics . . . 5
Aβ Fibril structure and polymorphism . . . 6

Methods **9**
Ion-exchange chromatography . . . 9
Size-exclusion chromatography . . . 9
Ultraviolet-visible spectroscopy . . . 10
Circular dichroism . . . 11
Fluorescence spectroscopy (Thioflavin T assay) . . . 13
Transmission electron microscopy (TEM) . . . 14
Fibril measurement in TEM . . . 15
Surface plasmon resonance . . . 16
Mass spectrometry and crosslinking . . . 17
Kinetic analysis . . . 18

Results and discussion **21**
Paper I . . . 22
Paper II . . . 24
Paper III . . . 27
Paper IV . . . 29
Paper V . . . 31

Paper VI 33
Concluding Remark **35**
References **37**

Popular science summary

As our knowledge of diseases and the development of new technologies increases, many health problems that were lethal in the past can now be cured. Couple this to better life quality and improved medical care, we are seeing an increase in the average life expectancy. The downside to this, however, is that diseases that develop with age are becoming more common. There is currently an estimated 47 million people living with dementia with this number predicted to be doubled every 20 years. Alzheimer's disease (AD) accounts for 60-70% of all the dementia cases in the whole world. Most of the AD cases are sporadic and patients develop symptoms after 65 years of age. A small subset of all AD cases are caused by a modified gene that can be passed through generations and lead to the development of dementia at a much younger age. Patient with AD usually have memory and mental problems and become totally dependent on others in their late stage. Unfortunately, there is still no therapy available for AD on the market.

The hallmarks of AD are plaques and tangles in the brain which are believed to lead to the death of nerve cells in the brain. The plaques mainly contain fibrils that are formed by a small protein called amyloid beta (Aβ). Aβ has a tendency to clump (aggregate) together and form long fibrils. Many studies suggest that Aβ aggregation links to the development of AD, which is supported by cases of people with genetic modifications. Those modifications lead to an increased production of Aβ or more aggregation favoured products and are linked to an earlier development of AD symptoms.

How Aβ causes cell death is not known, but it is believed that the toxic species are not the fibrils but aggregation intermediates, made up of two or more Aβ peptides. To figure out the link between Aβ peptides and AD, aggregation behaviour of Aβ is, therefore, an important question. Chemical kinetics is an area of chemistry in which the reaction speed of a chemical process is studied. Specifically, in aggregation kinetics, the detailed reaction steps and rates of the formation or disruption of a complex is studied. The overall aggregation process can be divided into several steps. This process can be thought of as standing in line at the supermarket. If we consider the people to be Aβ a long line of people would represent a mature Aβ fibril. To form the line, only a few people are needed and generally stand close to each other at the check-out, which is referred to as primary nucleation. The nucleus then grows as more people join and the line becomes longer, a process termed elongation. As more and more people join the line, there forms a long queue, which in our case is the mature fibril. As the line grows, people try to cut in by standing off to the side of the line (secondary nucleation), should a neighbouring cashier comes to work, this group of people (new nucleus) are in prime position to break off from the line (fibril)

and start queuing at the front of a newline, thus the process repeats and a new line (fibril) is formed. This queuing example is used here only to explain the simplified basic steps in the Aβ aggregation. The general supermarket would not have the capacity to open enough cashiers to cope with massive secondary nucleation that is involved in the aggregation kinetics. In reality, the fibril surface serves as a very efficient catalyser that helps to generate a huge amount of Aβ oligomers, which is then followed by elongation to produce more fibril surface. These processes form a catalytic cycle that boosts the Aβ fibril formation and is potentially very dangerous to the brain.

Our study is mainly focused on solving the aggregation mechanism of Aβ . In my work, we use experimental tools to follow the aggregation of Aβ and its gene modified variants that link to early-onset AD, Aβ with different length, or at different pH or salt concentration. The experimental data was then analysed using mathematical equations to find out the detailed steps that are involved in the aggregation. We found that some gene factors and environmental factors lead to a decreased repulsive force between molecules. Thus, the clumping between molecules or with bigger complexes is favoured. The saturated secondary nucleation is observed in all these cases, which means the catalytic fibril surface (queue) is fully covered by monomer (people), and new nuclei formation speed is limited by the release of the nuclei from the catalytic surface. In this case, the secondary nucleation speed is reaching the maximum. This secondary nucleation speed maximization leads to massive amount of oligomer production, which is potentially a high-risk factor to the brain. A chaperone protein, Brichos, is found to selectively hinder this secondary nucleation and drastically decreases the toxic oligomer production.

Overall, our study reveals the kinetic details of Aβ aggregation, mainly focusing on the effect of intrinsic and extrinsic factors. We have identified that secondary nucleation is the critical pathway that generates toxic oligomers and as such could be an important target in the development of effective therapy for Alzheimer's disease.

论文简介

阿兹海默症 (AD), 也就是人们口中常说的老年痴呆症, 是失智症中最主要的一种病, 大概占到失智人群总数的 70%. 此病多发于 65 岁以上的老年人, 发病后会出现记忆力, 思考力, 行动力的退化. 随着病情的恶化, AD 晚期的病人生活不能自理, 需要完全依赖他人的照顾.2015 年的全球失智症报告指出, 预计到 2050 年, 世界罹患此病的总人口将达到 1.3 亿. 在中国, 得益于经济的飞速发展, 人们的生活水平和社会医疗技术水平不断提高, 从而带来了人均寿命的大幅增长. 随之而来的一系列与人口老龄化相关的问题将变得异常突出. AD 作为一种常见的老年慢性病, 因其病程长并且暂无有效的药物治疗, 会给家庭和社会带来沉重的压力.

AD 的主要病征是脑组织内出现的斑块以及大量死亡的脑细胞和缩小的脑容量. 科学家推断这些斑块跟 AD 病人的脑细胞的死亡有很大的关联. 老年斑块的主要成分是一种叫做 β-淀粉样多肽 (Aβ) 的蛋白质. 导致阿兹海默症的病因至今依然存在很多争议. 其中最主要的论断是这种 Aβ 的聚合产物对脑细胞产生毒性进而导致了 AD. 这一论断被几种不同类型的痴呆症所支持. 比如, 临床上有些病人因为携带特殊基因而致使 Aβ 过量产生, 最后导致痴呆症的早发, 如唐氏综合症.

蛋白质是由氨基酸连接而成的多肽链, 是人体非常重要的组成部分. 人体的各个器官及其功能的维持, 诸如吃饭, 运动, 睡觉等等, 都离不开蛋白质. Aβ 蛋白存在于每个人的身体里, 在独立的状态下是没有毒性的. 但是很多个 Aβ 蛋白容易聚集在一起, 形成条形纤维. 这种纤维存在于脑神经细胞之间, 它们的堆积就形成了前文所提到的在 AD 患者脑部发现的斑块. 起初大家把这种纤维跟脑细胞的死亡联系到一起. 然而, 近年来的研究结果表明 Aβ 聚合过程中, 由几个 Aβ 聚集而成的小型复合物 (低聚物) 才是真正的有毒种类. 因此, 研究 Aβ 聚集与 AD 的关系成为很多科学家的研究目标, 旨在找到有效的抑制有毒性的 Aβ 低聚物产生的办法, 从而有针对性的减少甚至消除 Aβ 低聚物的产生, 抑制其对大脑的损伤.

本论文的主要目的是研究 Aβ 的聚合步骤. 我们通过改变内部因素 (Aβ 自身) 和外部因素 (溶液环境), 观察其对 Aβ 聚集的影响. 关于内部因素的研究具体有两点: 1. 氨基酸序列不同的 Aβ 突变体. 这些突变体通常跟早发的遗传性阿兹海默症有关 (< 65 岁). 2. 不同长度的 Aβ. 人体内最普遍的 Aβ 蛋白有两种, 含 40 个氨基酸的 Aβ40 和含 42 个氨基酸的 Aβ42, 它们共同存在于人体内, 并且都易于聚合. 对于外部因素的研究, 我们主要测试了溶液的盐浓度和溶液酸度的变化, 以及外来蛋白对 Aβ 聚合的影响.

Aβ 的聚合机理可以整理成一个较为简单的例子. 如果将 Aβ 比喻成在超市购物准备结账的人们, 他们三三两两的站成一个个称为核的小团体. 成核过程会产生 Aβ 低聚物, 最终排成的稳定整齐的长队就是条形纤维. 早

上超市刚开门, 大家陆陆续续开始去结账. 一开始只有一两个人在结账, 他们站的很近, 相当于聚合机理里的初次成核. 接着出现了第三个人, 紧排在前两人身后, 此过程可以看作是延长反应. 后续的人越来越多, 站成长队就形成了条形纤维. 此时有个人买好东西过来结账时看到队伍很长, 想插队早点结账. 于是拉上一个与他相熟的人在队伍的中间贴着队伍站, 开始边聊天边等待. 此时的状态, 他们两个在队伍表面形成的新的小团体相当于二次成核. 恰巧在这时, 旁边的收银员来上班了, 这两个人眼疾手快立马去了隔壁收银台, 成为了一个新核. 陆陆续续又有人在她们后面延长反应, 形成的新的队伍两旁又有人来插队 (二次成核), 接着插队的人又去了新开的收银柜台, 以此类推, 形成了一条条新的队伍 (纤维). 这个例子只是简单的描述了 Aβ 聚合的基本步骤. 实际情况下普通超市大概不会有很那么多人插队 (二次成核), 超市也没有办法提供新的收银柜台给所插队的人 (新核脱离纤维). 而 Aβ 纤维可以催化新核在表面的形成, 产生大量的低聚物. 而低聚物脱离母体纤维, 与其它的 Aβ 通过延长反应所形成的纤维又会催化产生更加大量的低聚物. 这个反应形成了一个循环, 大大加速纤维的生长和有毒低聚物的形成速度. 也就是说, 二次成核是聚合过程中的关键步骤, 可能是对脑细胞造成威胁的重要原因.

在具体的研究中, 我们加入了一种可以跟 Aβ 纤维特异性结合并发出荧光的分子, 在 Aβ 聚合过程中, 通过仪器检测发光强度, 对样品中 Aβ 纤维的生成数量进行跟踪. 然后加上理论分析, 用数学模型模拟这些聚合反应, 并与真实的实验结果对照, 找出 Aβ 聚合的具体路线和速率. 通过我们的研究发现, 二次成核是 Aβ 聚合过程中占绝对的主导地位, 是产生有毒低聚物的重要原因. 通过改变内因, 我们发现早发遗传性 AD 的突变体 Aβ 聚合的速率比普通的 Aβ 聚合要快, 并且在二次成核这一步达到了速率极限. 这暗示了突变体携带者的体内有大量的有毒低聚物产生, 它们会对大脑进行快速的侵蚀. 这与突变体基因携带者大多数会在五十岁左右甚至更早出现 AD 的症状相吻合. 将外因改变后我们观察到, 在增加溶液盐浓度, 降低酸度的情况下, 同样的二次成核达到极限速率. 而我们的另一项研究发现, 在聚合体系中加入分子伴侣蛋白 Brichos 可以专门抑制 Aβ 的二次成核, 从而大大减少低聚物的产生, 降低对细胞的毒性.

综合以上结果, 我们的实验和模型有助于实现通过改变某些因素, 定向选择并影响特定的 Aβ 聚合步骤. 这一手段也许能够被 Aβ 治疗方法所利用, 比如定向抑制二次成核, 减少有毒低聚物的产生. 治病讲究对症下药, 只有发现了问题症结之所在, 才能找到正确的解决办法. 本论文的研究仅仅是针对阿兹海默症的研究中的一个小环节. 仅以此论文作为一块小小的垫脚石, 为此病症后续的研究提供一些参考和借鉴. 希望未来有一天, AD 不会再给人们带来病痛和悲伤.

Acknowledgements

For all these five years in Lund, I enjoyed living in this calm and lovely university town. Being a PhD student has been both challenging and rewarding and I am very glad to see that the part I could not imagine before, is happening now. There are so many people that I want to say thanks, thanks for being a part of my PhD student life, thanks for your sharing and caring when I experience ups and downs, thanks for the greetings every day, and thanks for all the cheering and supporting.

Sara, I am really appreciating that the day you answered 'yes' to me and offer me the chance to do PhD candidate work in your group. You are the best supervisor ever. Thanks for showing me all the experimental procedure on the very first day, I was so surprised and almost shocked that you were teaching me all the details, which is so different from my previous experience. Not until later I realised that surprise was just the beginning. I cannot describe how much you have influenced me. I am feeling grateful for your persistent invitation every year for the Sankt Hans Extreme (SHE) race and I, from not being able to run 200 metres non-stop, now have accomplished two 5 km SHE. You inspired me to try something that I have always been thinking but not dared to try. Thanks for being so helpful and supportive during this whole time, I am so lucky to have you as my supervisor. **Tommy**, thanks for your advices and feedback on my project work, for always being helpful, supportive and also for organizing so many fun group activities. **Emma**, thank you for the discussion and feedback in all kinds of presentation.

To our group members, it has been a great pleasure working with you. **Birgitta**, thank you for being patient with all my questions about work and life, also thank you for sharing your music and happy moment. **Kalyani**, thanks for being a helpful colleague and a close friend like family, you are always so kind to share and help. **Tanja**, thanks for being supportive and always be there when I have any question. **Karin**, thanks for coming to my wedding and now after this whole thing we finally can start driving! **Martin** and **Celia**, thanks for your help in experimental work and group meeting discussion. **Ricardo**, thanks for offering me help and the driving tips. I will soon start to try it. **Janina**, thanks for all the nice chats and invitation to tango. **Matthias**, thanks for all the discussions and your courage to try 'weird and scary' snacks that I offered. **Thom**, thanks for being a kind officemate and sharing the running tips and fun stories. **Katja**, thanks for being so patient and helpful in the lab. **Chris**, thanks for organising the journal club and your help in this work. **Tinna**, thanks for being a good friend, a teacher, a lab-mate, I enjoyed a lot of working and hanging out with you. Thank you for all your support during my thesis time and sharing your music to lift me up. **Stefan G**, thanks for all the chats and organising the hiking trip. I really wish I could go. **Veronica L**, thanks for

sharing your smile. I miss you and want you back. **Ilaria**, thanks for being a nice company both in biochemistry side and physical chemistry side. Every small talk during the thesis time helps. **Eimantas**, thanks for being so helpful in the lab and for the nice chats during fika. To our previous group members, **Eva T**, thanks for preparing the experimental material. **Risto**, thank you for the nice collaboration in our co-aggregation story, and the music and fun video you shared. **Jonas**, thanks for all the chats and the ghost chili. **Olga**, **Erik** and **Elodie**, thanks for all the help and support, great chats, and for sharing your knowledge and time. I have learned a lot from you.

To our collaborators, it has been great experience of working with all of you. **Georg**, **Tuomas**, **Chris**, **Sam**, **Ulrich**, thank you all for your input in the excellent collaborations and fruitful discussion. **Clemen** and **Laurie**, thanks for hosting me in your lab to do STORM imaging. **Jenny P**, **Henrik B** and **Jan J**, thanks for providing Brichos sample and advices on protein purification.

To people in the department, **Cecilia M** and **Cecilia E**, thanks for the nice collaboration and scientific discussion, and also the very good apple pie. **Ingemar**, thank you for your supports, especially during the thesis time. **Gunnel**, thanks for running TEM samples and always being so helpful. **Adine**, **Magnus**, **Tobias** and **Susanna**, thanks for your help in all kinds of practical problems. **Ingrid**, thank you for spending time helping me with the practical paper work. Big thanks to all the friends in CMPS, **Andreas**, thanks for asking me to join the badminton, and also for being a caring and thoughtful friend. **Henry**, thanks for your patient and tolerance and always being there as a great company. **Yonathan**, thanks for sharing your knowledge in crystallisation and also for sharing the ski experience. **Aaron**, thanks for being so supportive all the time. **Irem** and **Elli**, whenever I think about you, I feel warmth in my heart. Thanks for being a sweet friend. **Alak**, thanks for caring and being supportive all the time. **Johan W**, thanks for all the odd but fun discussion. **Olof**, **Bhakat**, thanks for asking me to join fika. Now it will happen more often. **Eva-Christina**, **Robert** and **Eva S**, thanks for all chats and nice cakes. **Erik H**, thank you for sharing your philosopgy in running. **Jenifer**, **Sumitha**, **Sabeen** and **Lavanya**,thanks for nice chats and greetings from time to time. **Veronika N** and **Stefan K**, thanks for organising the beer club and BBQ. **Luigi**, thank you for being so 'mean' to me and you are my favourite Italian. **Janne F**, thank your for all the nice chats during lunch and for the diving inspiration. **Dat**, thank you for all the fun chats and tasty Vietnamese food.

To my friends outside Kemicentrum, **Stenni**, thanks for all the cocktails, plum wine and all the happy time together. **Sinéad**, thanks for the fun time we have spent together. **Romany**, thanks for the time in Lund and also for meeting me in LA. We surely will meet again. **Suticha**, thank you for being a great friend and for the great

hospitality in Thailand. **Chialing** and **Lubi**, thanks for the fun time we shared in riding and in handcrafting. **Samia**, I miss the days baking and playing tennis with you. Come back!!! **Fredrik**, you are my very first Swedish friend and the language teacher, thanks a lot for introducing me to your homeland. **Gunilla**, thank you for being such a nice great teacher.

Lastly, I would like to spend a few words to express my appreciation to my parents and friends in China and Chinese friends in Lund. You made it like home.

在这个部分，我首先要感谢亲爱的爸妈，不管走到哪里，你们永远是最我坚实的依靠．谢谢你们给我的爱和教养，你们的牺牲和你们的理解，让我能够安心的做自己想做的事．谢谢我的叔伯亲人们，感谢你们的信任和支持，正是因为有这个互帮互助的大家庭作后盾，我才能无后顾之忧的踏上跨洋过海的求学之路．非常感谢我的两个朋友，刘月茹和张丽，感谢你们陪我走过这长途旅行前的一段苦旅，开心有人分享，开心便加倍了；麻烦有人分担，麻烦就更容易被解决掉．最后我要感谢我的先生，我们是如此不同个性的两个人，在十年的相处中慢慢磨合，一起蜕变．感恩当初分隔两地的坚守与执着，感谢十年经历的各种低谷时的陪伴和支持，谢谢你在我犯懒的时候默默洗碗做饭把我喂饱．感谢你陪我走过博士生最挣扎的时光．最后我要谢谢在隆德的一众好友们．芮羽王健夫妇，去你家吃零食看暴走聊天是最减压的时候．宏多和彭飞以及嘟嘟和妞妞，感谢每次求蹭饭都有求必应而且都是一桌子菜加上一对萌娃陪吃饭陪玩好治愈．还有一众隆德的朋友，知非，熊妈妈，璇璇和虹虹，常总，小姜姜，伤不起，得朋儿，光头哥，飞哥，你们在我的让我在隆德的生活像家一样．在隆德的记忆正是因为有了你们才更加的饱满．不管以后在世界的哪个角落，我永远爱你们，么么哒．

List of papers

I **Aggregation mechanism of Aβ42 familial mutants resolved over microscopic steps**

Yang X, Meisl G, Frohm B, Thulin E, Knowles T and Linse S
Manuscript

II **The Aβ40 and Aβ42 peptides self-assemble into separate homomolecular fibrils in binary mixtures but cross-react during primary nucleation**

Cukalevski R*, **Yang X***, Meisl G, Weininger U, Bernfur K, Frohm B, Knowles T and Linse S.
Chem. Sci. 2015; 6:4215-33.
* Contributed equally

III **A molecular chaperone breaks the catalytic cycle that generates toxic Aβ oligomers**

IV. Cohen SI, Arosio P, Presto J, Kurudenkandy FR, Biverstål H, Dolfe L, Dunning C, **Yang X**, Frohm B, Vendruscolo M, Johansson J, Dobson CM,Fisahn A, Knowles TP, Linse SS. Linse
Nat Struct Mol Biol. 2015, 22(3):207-13.

IV **Differences in nucleation behavior underlie the contrasting aggregation kinetics of Aβ40 and Aβ42 peptides**

Meisl G, **Yang X**, Hellstrand E, Frohm B, Kirkegaard JB, Cohen SI, Dobson CM, Linse S, Knowles TP
Proc Natl Acad Sci USA 2014;111:9384-9.

V **Quantitative analysis of intrinsic and extrinsic factors in the aggregation mechanism of Alzheimer-associated Aβ peptide**

Meisl G, **Yang X**, Frohm B, Knowles T PJ, Linse S
Scientific reports. 2016; 6:18728

VI **Modulation of electrostatic interactions reveals a general reaction-network to unify the aggregation behaviour of the Aβ42 peptide and its variants**

Meisl G, **Yang X**, Dobson C, Linse S, Knowles T
Submitted to Nat. Chem. Bio

All papers are reproduced with permission of their respective publishers.

My contribution to the papers

I I performed concentration-dependent aggregation experiments, seeding experiments and sample preparation for TEM imaging for all five mutants. I also performed protein expression for one mutant and purification for two mutants I also did preliminary data analysis and wrote the first draft of the manuscript.

II RC and I performed all experiments including aggregation kinetics, self-seeding and cross-seeding aggregation kinetics, TEM sample preparation, MS measurement and data analysis. I wrote part of the paper and contributed to the revision.

III I prepared sample for TEM imaging. I wrote the corresponding part in the paper and participated in the revision of the paper.

IV I performed the seeding experiment for elongation rate estimation and prepared the sample for TEM imaging. I also contributed to the paper writing.

V I performed the Aβ42 wt aggregation kinetics at pH 7.4 and prepared samples for TEM imaging at pH 8.0 and pH 7.4. I contributed to the paper finalization.

VI I performed part of the kinetic test and prepared samples for TEM imaging. I contributed to the paper revision.

List of abbreviations

ACH	Amyloid cascade hypothesis
Aβ	Amyloid β
AD	Alzheimer's disease
APP	Amyloid precursor protein
CAA	Cerebral amyloid angiopathy
CD	Circular dichroism
E. coli	Escherichia coli
FAD	Familial Alzheimer's disease
IEC	Ion-exchange chromatography
MALDI	Matrix-assisted laser desorption ionization
MS	Mass spectrometry
NMR	Nuclear magnetic resonance
Phe	phenylalanine
PSEN	Presenilin
SEC	Size-exclusion chromatography
SPR	Surface plasmon resonance
TEM	Transmission electron microscopy
ThT	Thioflavin T
TOF	Time of flight
Trp	Tryptophan
Tyr	Tyrosine
UV	Ultraviolet-visible

Introduction

Alzheimer's disease and amyloid β peptide

Alzheimer's disease (AD) is the most common neurodegenerative disease that accounts for 60-70 % of the cases in the world.[1] Most of the AD cases are sporadic with an average onset age around 65. Patients gradually have problems on their memory, thinking and behavior. A small subset of the cases are hereditary forms called familial Alzheimer's disease (FAD) with gene mutations and most of these cases are linked to an early-onset AD, which develop the disease in a very similar pattern but at a much younger age.[2] The disease is progressing a long period before the symptoms manifest. Due to the lack of effective treatment, a patient who is diagnosed with AD is not possible to get the pathology reversible. Nowadays, millions of people are suffering from AD and this number will almost be doubled every two decades.[3]

Pathology of Alzheimer's disease

AD develops as the result of a complex series of events that take place in the brain over a long period of time. In the comparison of a healthy brain and a brain with advanced AD, the sick brain volume has a dramatic shrinkage, which is especially severe in the hippocampus area that is involved in short and long-term memories and spatial orientation. Extracellular senile plaques and intracellular neurofibrillary tangles are found to deposit and spread through the cortex as AD is progressing. Additional pathology includes synaptic degeneration, neuronal cell death, mitochondrial dysfunction, etc.[1,4] The senile plaques are mainly composed of misfolded amyloid β (Aβ) fibrils and are present between neuron cells. Tangles are mainly formed of tau protein aggregate and are found intracellularly in the dead or dying nerve cells. Though there have been studies about AD for many decades, there is still no concrete conclusion about the cause of the disease.[5] Among all proposed

theories, the Aβ peptide, which is involved in the senile plaques, wins the most support (Fig. 1).

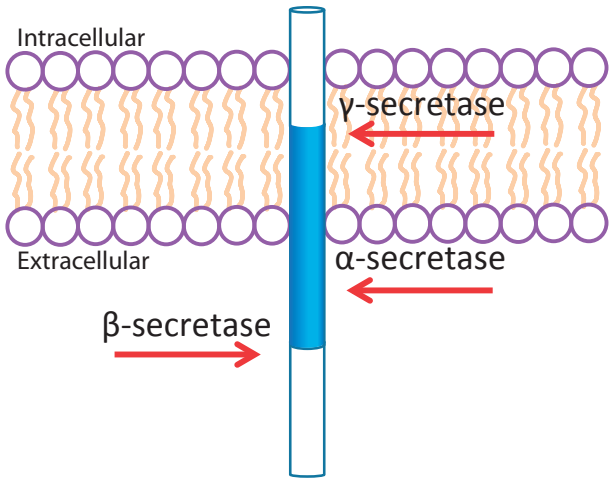

Figure 1: APP enzyme cleavage site by β-secretase, α-secretase and γ-secretase. The blue part is the Aβ peptide that would be released in the amyloidogenic pathway.

Amyloid cascade hypothesis

In 1992, Hardy and Higgins proposed a theory behind the pathogenesis of AD that is well-known today as the amyloid cascade hypothesis (ACH).[6] It is proposed that the deposition of Aβ fibrils as a form of senile plaque is the main reason that leads to AD pathology and all other pathologies are followed as a downstream effect, e.g. neurofibrillary tangles, neuronal cell death, vascular damage and ultimately dementia. There are a few observations that support the ACH. Firstly, the deposition of Aβ fibrils in the senile plaques;[7,8] secondly, mutations in the APP gene and presenilin (PSEN) 1 & PSEN2 genes; lastly, trisomy of the chromosome 21 in Down's syndrome. This genetic factors lead to either increased total Aβ production or a higher Aβ42/Aβ40 ratio,[9] which is linked to the early-onset of AD symptom (< 65 years).

Since many cases that with gene modifications and sporadic AD form have a very similar phenotype, it was believed that the higher gene dosage and mutations alter the Aβ expression pattern, generate a higher ratio of Aβ42/Aβ40, or create more aggregation prone Aβ variants that lead to faster deposition of Aβ fibrils and accelerate AD progression.[10]

Amyloid precursor protein and amyloid β peptide

Amyloid precursor protein (APP) is a transmembrane protein and its physiological function is not entirely clear. However, APP is considered to be involved in cell adhesion, neurite outgrowth and synaptogenesis.[11] APP is mostly well known for its the connection to AD. APP can be cleaved by secretases, which generates Aβ peptide fragments (Fig. 2).[12,13]

In the non-amyloidogenic pathway, APP is processed within the Aβ region by α-secretase and γ-secretase to generate a 3kD peptide called p3 that is not involved in the disease. In the amyloidogenic pathway, APP is cleaved by β-secretase and γ-secretase, which produces an aggregation prone peptide that is called Aβ peptide.[14,15] β-secretase cleaves at the N-terminus of Aβ and γ-secretase cleaves the C-terminus, which generates several Aβ variants that differ in length.[16] The processed peptide of 40 amino acids (Aβ40) is the most abundant variant from the cleavage and the variant of 42 amino acids (Aβ42) is more hydrophobic (additional alanine and isoleucine on the C-terminus) (Fig. 2) and more toxic.[17,18] In a sporadic case, Aβ40 and Aβ42 are presenting with a ratio of 9:1 in cerebrospinal fluid, whereas in cerebral senile plaques, Aβ42 is found to be the initial and main component, followed by deposition of Aβ40 during the development of the disease[19].

Figure 2: Aβ peptide sequence. Aβ40 and Aβ42 differs in the C-terminus of the peptide by two amino acids with hydrophobic side chains. The charge of the amino acid at a pH in the physiological relevent range is shown below the sequence. At this pH range, the three histidines are titrating.

In this thesis, recombinant Aβ peptide with a methionine as the first residue, due to need for an ATG start codon, is produced to guarantee the purity and sequence homogeneity, which is crucial for reproducible kinetic analysis[20]. The sequence of Aβ is presented in Fig. 2 with charges shown in below. The two main variants, Aβ40 and Aβ42, have a net charge around -3 to -4 at physiological relevent pH. Aβ peptides show random coil structure in the native state. But at the physiological conditions, this peptide has a tendency to aggregate and form fibrils that contain β-sheet secondary structure.[21] Initially, mature fibrils are thought to be the toxic species that is involved in the disease. However, later studies have found that the Aβ

oligomeric state has much more enhanced neurotoxicity than the final product.[22–25]

Early-onset familial Alzheimer's disease

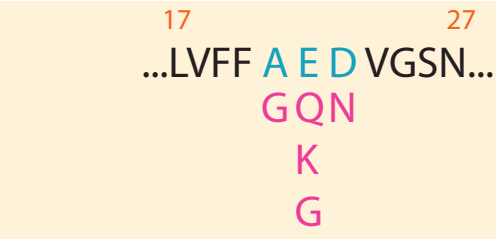

Mutants	Absolute charge reduction
A21G (Flemish)	0
E22G (Arctic)	1
E22K (Italian)	2
E22Q (Dutch)	1
D23N (Iowa)	1

Figure 3: Aβ mutations on site A21 to D23. The absolute charge reduction is shown in the table below.

FAD is defined as an AD type with symptoms that manifest in a familial trend and could be passed through generations. FAD is caused by missense mutation in PSEN1, PSEN2 and APP genes.[8,26,27] The peptide product of PSEN1 and PSEN2 are located in the catalytic core region of γ-secretase and influence the Aβ cleavage at the C-terminus,[15,28] which leads to an increased Aβ production.[9,29] The mutations in APP close to the cleavage site affect the product length and population that is released by the enzymes.[15] Mutations in the Aβ region lead to generation of an Aβ segment with different aggregation propensity. All of these factors lead to production of more aggregation-prone Aβ peptide, varied peptide population, or altered Aβ40/Aβ42 ratio and are related to an onset of the AD or similar pathology manifests at around 50s.[2,30–32] Several studies on the plaque component agree that these mutations lead to the increase of Aβ42 and Aβ42 is the dominant form in the senile plaques.[33,34]

In this work, we are mainly focus on the familial mutations of APP and the mutations studied are on site A21-E22-D23 in the Aβ region. The mutants are name as A21G(Flemish), E22G(Arctic), E22K(Italian), E22Q(Dutch), D23N(Iowa) These familial mutants lead to development of symptoms at a much younger age of ca.

40-50. Some of these mutants (A21G, E22Q and D23N) develop pathologies of severe CAA combined with cognitive decline. CAA is led by the deposition of Aβ peptide on the wall of blood vessel in the central neural system and usually results in additional pathologies such as cerebral haemorrhage, stroke, leukoencephalopathy and cortical calcification other than the conventional pathology.[35–38] It is found that Aβ40 is the major species that is found deposit in vessels in CAA while both Aβ40 and Aβ42 are present in plaques.[34] These mutants are the most well studied APP mutants[10,39–42] but there is lack of systematic kinetic analysis of the aggregation mechanism.

In this study, our primary interest is to investigate the effect of mutations in the central region on the aggregation mechanism and its link to the amyloid deposition. The familial mutations in site A21-E22-D23 cause an absolute charge reduction of 1 to 2 unit and the peptides with these mutations are shown to be more aggregation prone in several APP mutant studies.[20,31,43]

Aβ aggregation kinetics

Aβ peptide is a natural protein that is expressed in all human bodies. The monomeric form of Aβ is causing no problem but the peptide has a tendency to self-assemble and form highly ordered β-sheet rich structure, a so-called 'amyloid structure' . The oligomer species that is produced during the aggregation is now considered to be the neuronal toxic species.[22,24,25,44]

Aβ aggregation kinetics has been extensively studied during the past decades[45–47] and the overall self-assembly reaction is composed of several microscopic steps: primary nucleation, where a nucleus is formed by monomer assembly; elongation, in which the monomer can associate at the end of a fibril; secondary nucleation, a process to generate new nuclei and is catalyzed by the fibril surface; fragmentation, where a fibril breaks and produces new ends for monomers to elongate. The primary nucleation rate is relatively slow due to a high free energy barrier, which yields a long lag phase in the aggregation when followed by using Thioflavin T (ThT) as a fluorescence probe (Fig. 7). Oligomers are transient species, the structure of which undergoes structurally reorganization to reach a more ordered state.[48] Followed by elongation, the peptides associate into fibrils, which can generate longer fibril that can be used to catalyse the formation of more nuclei on the surface. The secondary nucleation rate usually is much higher than that of primary nucleation[45,49,50] and boost the production of nuclei, which leads to an exponential growth of the fibril mass. The secondary nucleation rate is dependent on monomer concentration and also found to reach a saturated situation of which the rate is not depending

on the monomer association onto the fibril surface but rather on the dissociation of the newly formed nuclei. This is observed so far in a few cases, e.g. increase in peptide concentration, screened electrostatic repulsion by adding salt, weakened electrostatic repulsion from point mutation that is less charged, or increase in hydrophobicity that favours the molecular interaction.[20,50,51]

Aβ Fibril structure and polymorphism

Many proteins with quite a diverse amino acid sequences can form amyloid fibrils.[52] Those fibrils are composed of mainly β-sheet and typically contains several protofilaments that wind around each other.[53] The fibril structure has a distinct cross-beta pattern that was firstly discovered in 1935. Fibrils formed by egg-white was diffracted under an X-ray beam. The diffraction pattern showed a 4.8 Å spacing between β-strands within the β-sheet and roughly 10 Å between the β-sheets.[54,55] The β-sheet lies perpendicularly to the long axis of the fibril, and stacks along the fibril growth direction. The hydrogen bonding between the stacked β-sheet is parallel to the fibril long axis and the side chains are pointing to the inside or outside of the fibril core. It is proposed that the fibril structure is stabilized by the interaction between the side chain groups as well as the hydrogen bonds between peptide backbones.[56,57]

Amyloid fibrils exhibit pronounced structural heterogeneity when observed under microscope, e.g. varied periodic twist distance, fibril thickness, different curvature, which implies a polymorphism of amyloid fibrils.[58–61] Aβ polymorphism has been reported in a few studies for different Aβ variant.[61–65]. One example is that 12 different morphologies have been identified for Aβ40 fibrils using TEM in combination with 3D image reconstruction.[66] This polymorphism has also been observed *in vivo* and found that the fibrils taken from the brain of two different patients catalyse the formation of different fibril structures when used as seeds.[67] Although the full-length Aβ fibrils structure is not resolved in an atomic detail, and there has been no success in full-length Aβ crystallization, small segments of Aβ peptide are found to be able to form microcrystals and the structures have been determined using X-ray diffraction[68,69]. The result shows that the residues of two neighbouring peptide side chains are packed sterically in register and form a 'steric zipper' motif. The detailed structure shows that different in-register side chain packings, with β-strands running parallel or antiparallel, are observed in crystals formed by the same segment. This packing diversity may provide the molecular basis for the Aβ fibril polymorphism.

Other experimental techniques, e.g. cryo-TEM, scanning TEM, electron param-

agnetic resonance, small-angle neutron scattering, X-ray fibril diffraction as well as nuclear magnetic resonance (NMR) are used to determine the fibril structure.[21] Several models that are determined using these approaches suggest that Aβ protofilaments are composed of a two or three folds of β-strand-turn-β-strand motif, a hairpin-like folding[21,70–76] with a 10-17 amino acids flexible N-terminus and a core region located C-terminus.[67,71]

Methods

Ion-exchange chromatography

Ion-exchange chromatography (IEC) is a method to separate proteins based on their net charges. The matrix of the stationary phase in IEC is composed of beads with negatively or positively charged groups, called cation-exchange resin or anion-exchange resin, respectively. The cation-exchange resin can be used to separate molecules with positive charge whereas the anion-exchange resin can be used to separate molecules with negative charge. The protein mixture containing the target protein when applied on the IEC column will bind to the resin with different affinity depending on the net charge. Then the proteins can be separated by washing the resin with increasing concentration of salt to compete binding to the charged group of the resin. Proteins with low net charges will be eluted first, followed by proteins with higher net charge.

Size-exclusion chromatography

Size-exclusion chromatography (SEC) is similar to IEC but separates molecules based on the protein sizes. SEC is sometimes referred to as gel filtration, as the beads used in the column are usually made of highly hydrated insoluble polymer, i.e. agarose, dextran or polyacrylamide. The polymer beads are structured with pores on the surface with a special distribution of pore size. After applying protein samples on the column, large molecules cannot get into the pores of the beads thus have a smaller volume to travel through the column, whereas smaller molecules can enter the pores thus migrate slower. Separation happens when molecules of different sizes pass through column and have different interaction time with the matrix. Consequently, larger molecules are eluted from the column first and then smaller molecules. Fig. 4 is an example of Aβ applied in SEC.

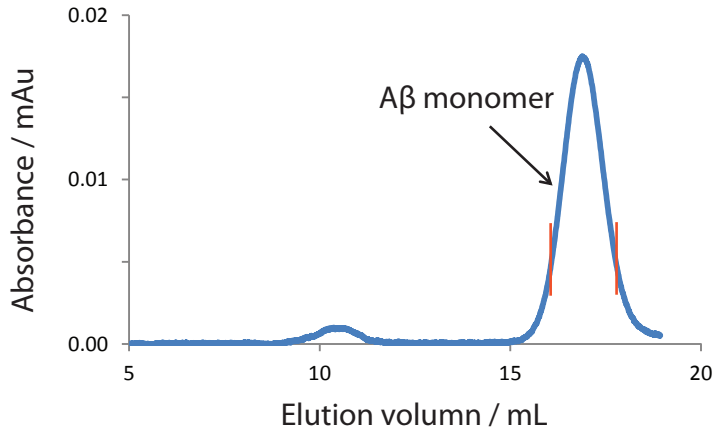

Figure 4: Aβ gel filtration (SEC) chromatogram. Aβ peptide is dissolved in 1 mL 6 M GuHCl solution and incubate at room temperature for 15 to 20 min before injection. The Aβ monomer is eluted at around 15 mL. Only the central part of the peak is collected and the concentration of the collected fraction is calculated as discribed in UV spectroscopy using Eq. 3.

Ultraviolet-visible spectroscopy

Molecular energy is composed of three parts, electronic energy E_e, vibrational energy E_v and rotational energy E_r, as formulated in Eq. 1.

$$E = E_e + E_v + E_r \tag{1}$$

Each electronic energy level has several vibrational energy levels and each vibrational energy level contains multiple rotational energy levels. Molecules with π-electrons or n-electrons can be excited by absorbing energy from the incident UV light and jumping to a molecular orbital of a higher energy level, so-called excitation from ground state to the excited state. The energy that is absorbed by the molecule must be equivalent to the energy difference between the two energy states.

Most proteins contain amino acids with aromatic ring such as tyrosine (Tyr), tryptophan (Trp) and phenylalanine (Phe) that absorbs UV light and this feature can be used as a means to measure protein concentration. The light source is from a deuterium lamp (near UV region, 150-400 nm), and a tungsten-halogen lamp (visible region, 400-800 nm). Protein is prepared in a buffer solution and by shining light to the sample, the transmitted light is recorded by a detector. Contribution of the background absorbance can be subtracted by measuring only the buffer solution.

The absorbance is calculated using the equation as described below as Eq. 2. I_0 is incident light, I is transmitted light.

$$A = log_{10}(I_0/I) \tag{2}$$

According to the Beer-Lambert law (Eq. 3), concentration c can be calculated if the light path length l, absorbance and the extinction coefficient ε is known.

$$A = \varepsilon cl \tag{3}$$

In the Aβ amino acid sequence (Fig. 2), there is only one Tyr and three Phe. Phe has a peak absorbance at around 250 nm while Tyr absorbs the most at around 280 nm. Although there are three Phe and only one Tyr in the sequence but due to a much lower molar absorbance of Phe, the absorbance at 280 nm from Tyr is used to estimate Aβ concentration. In our study, the value of the extinction coefficient of Aβ peptide is determined by amino acid analysis and used in all our Aβ studies.

Circular dichroism

Circular dichroism (CD) is a method used to detect protein structural information, i.e. secondary structure in far-UV and tertiary structure in near-UV. Protein solution is illuminated by a linear polarized UV light that can be considered as a sum of two circularly polarized lights. Due to the chirality of the peptide chain backbones, the left and right circularly polarized light will be absorbed differently. As a result, the light which comes out of the sample is polarized ellipitically. The shape of the ellipse is usually described by the ellipticity, θ.

$$\theta = \arctan(b/a). \tag{4}$$

a and b are the long and short axis of the ellipse, respectively.

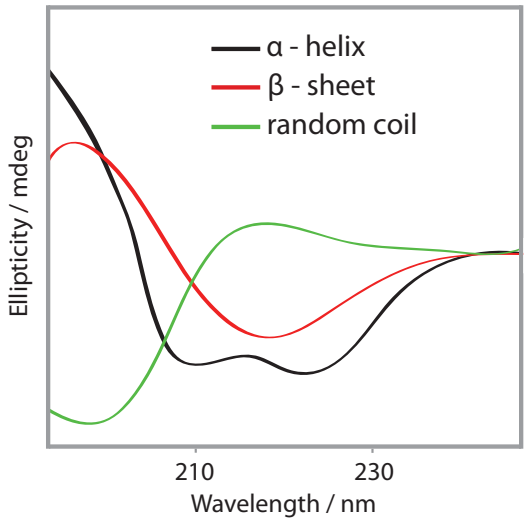

Figure 5: The typical CD spectrum of α-helix (black), β-sheet (red) and random coil (green).

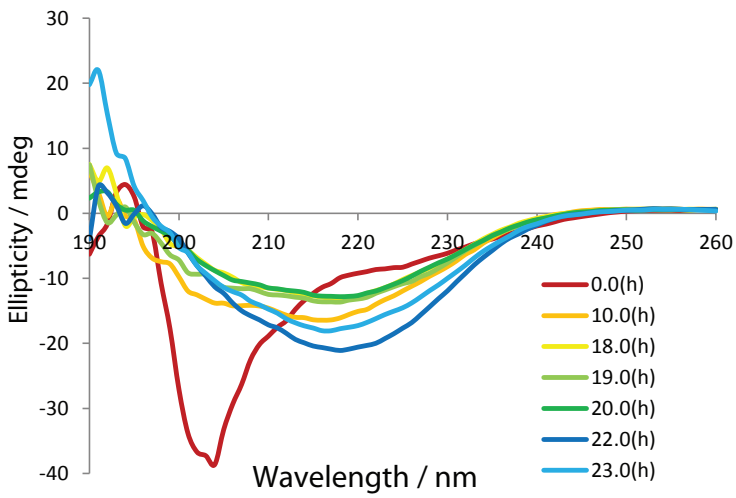

Figure 6: Aggregation of 10 μM Aβ40 was followed by CD as a function of time. Peptide structure with a conformational change from random coil (0 h) to β-sheet dominating structure (23 h). The decrease of ellipticity at 218 nm shows formation of β-sheet rich fibril structure.

The far-UV range is from 260 nm to 190 nm and the near-UV range is from 350 nm to 250 nm. The CD signal is mainly affected by the protein backbone in the

far-UV range and by aromatic groups and disulfate bonds in the near UV range but with low sensitivity. It requires a sample concentration of 0.1-0.4 mg/ml in a 1 mm cuvette for a far-UV and 1-2 mg/ml in a 10 mm cuvette for a near-UV measurement. CD is mostly used to study protein folding or conformational changes, e.g. time course measurement can be used to follow protein folding kinetics and temperature interval measurement can be applied to investigate protein denaturation. Typical CD spectrum of α-helix, β-sheet and random coil are shown in Fig. 5. Here in this work, CD is used to follow the formation of amyloid fibrils, which exhibits an enhanced β-sheet absorbance peak at around 218 nm (Fig. 6).

Fluorescence spectroscopy (Thioflavin T assay)

When a molecule absorbs light, the photons will promote electrons to travel to a different orbital, and the molecule is therefore excited from low energy ground state to an electronic excited state. Often the excited molecule is initially in a vibrationally excited state. In most molecules, the excited electron can travel back to the ground state again by giving away the extra energy in the form of heat. But for some special molecules, the electron can travel back to the ground state and falls back into the lower energy level by emitting a photon. These types of molecules are called fluorophores. Due to the relaxation in the vibrational level in the excited state, the energy gap between the ground and excited state that is given to the emitted photon is always smaller than the energy that the fluorophore has absorbed. Thus the emitting light always has a longer wavelength (lower energy).

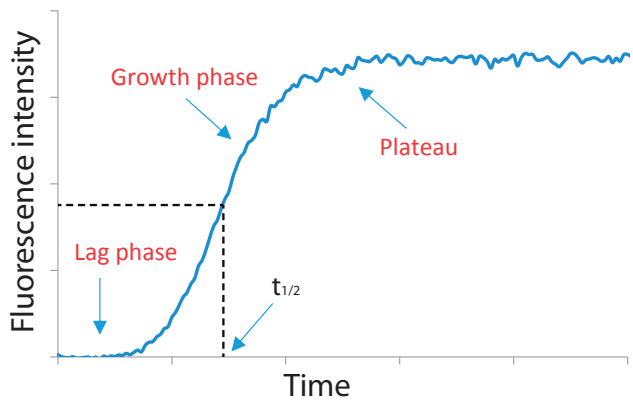

Figure 7: A typical sigmoial aggregation curve monitored by ThT fluorescence. The curve shows a flat lag phase, an exponential growth phase and a plateau. Half-time is defined as the point when ThT reaches half of the maximum intensity increase.

ThT is a fluorophore that binds specifically to a β-sheet rich region of a protein structure. It is commonly used in the field of studying the formation of amyloid fibrils. ThT can be excited at 440 nm and the emitting light is usually collected at 480 nm. After binding to β-sheets, ThT shows an enhanced fluorescent intensity which is proportional to the mass of fibrils (only accurate in a certain concentration range). By following the increase of the ThT intensity, one can monitor the amyloidogenic protein aggregation and even the aggregation mechanism can be resolved through global fitting to multiple ThT curves. In Fig. 7, a typical aggregation sigmoidal curve is shown, with a lag phase, a growing phase and a plateau.

Transmission electron microscopy (TEM)

In transmission electron microscopy (TEM), a beam of electrons is produced by an electron gun, which travels through vacuum in the column of the microscope and is then focused on the object. TEM uses electromagnetic lenses to focus the electrons into a thin beam and this electron beam travels through the object and interacts with the sample. During this interaction, some of the electrons are scattered and disappear. The unscattered electrons reach the base and hit a fluorescent screen, therefore, generate a monochrome image, like a shadow of the detected sample.

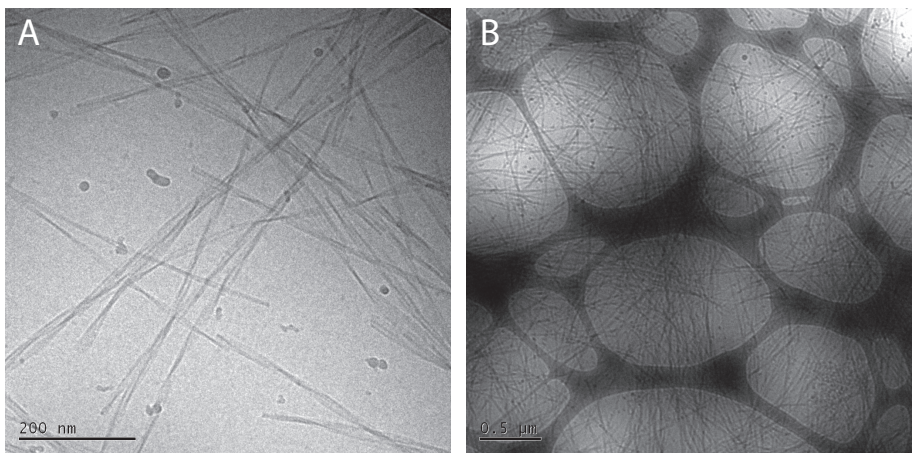

Figure 8: Aβ40 fibrils that is formed from 10 µM monomer. A) A close view of fibrils with a scale bar of 200 nM where one can see the fibrils with periodic twists. B) An overview of fibrils that form a net work or bundles. The scale bar is 0.5 µm.

There are mainly two ways to prepare the protein specimen for TEM. One way is called negative staining, in which the sample is dyed with a stain that contains heavy

metals and dried on the surface of a copper grid. The stain adsorbs to the biological sample and scatters electron strongly so as to generate better contrast in the final image. The drawback is that the sample needs to be dried, which means the native state of the protein is probably changed. To obtain high resolution images of the fibril morphology as in the originate state in solution, we use the cryogenic way to prepare our samples. In this way, the sample is prepared as a thin layer of ice (<100 nm) on a carbon filmed copper grid by flash-freezing in liquid ethane to prevent cubic ice formation and then stored in liquid nitrogen. In this way the sample can be fixed so as to reflect the original structure. The tricky part is to get a layer of ice that is thin enough to reach a good contrast.

Fibril measurement in TEM

One way to get quantitative information from the TEM image is to do the measurement in a graphic software. In our study, the Digital Graph software has been used to measure the fibril node-to-node distance (periodic twist distance). It is also possible to measure the fibril thickness.

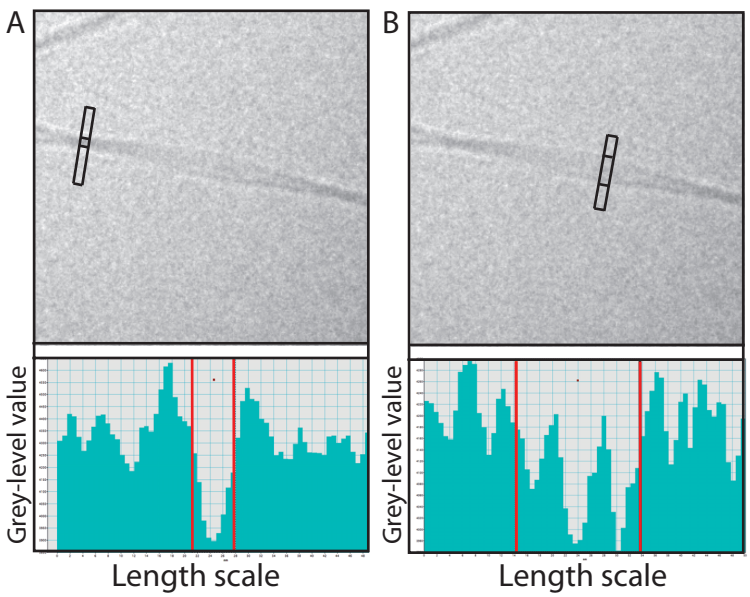

Figure 9: Fibril TEM image and the histogram profile of the gray-level value over the area that is marked. A) Fibril twist location. A sharp minimum intensity shown on the fibril twist. B) The multiple minima suggest the protofilaments that are involved in the fibril.

Such measurement helps to give a more direct result that is reflected in hundreds of images although it will not give a more precise number like as other diffracting or scattering methods. In the measurement, a histogram profile can be obtained by drawing a line on top of the object. This histogram profile reflects the gray-level value of the area marked. To get a more accurate calculation, the line must be lying vertical to the fibril axis and be expanded a bit along the axis. The fibril twist is defined where a single minimum intensity is found (Fig. 9A), which can be used to accurately locate the fibril twist position. Once the fibril twist is located, the periodic twist distance can be measured by drawing a scale on the histogram profile to mark the region of interest and a number is then given for this scale in the profile. As there is also background noise, the starting and ending point should be on the half-way of the slopes to have an averaged estimation. The multiple minimum intensity observed in Fig. 9B is due to the protofilaments that are involved in the mature fibril. The fibril length and thickness can be measured the same way.

Surface plasmon resonance

Surface plasmon resonance (SPR) is a method that can be used to study protein-protein and protein-ligand interactions. An incident light shoots on the back side of the sensor chip at a critical angle to generate full reflection and the reflected light from the surface is captured by a detector. During the reflection, a standing wave called evanescent wave is generated in the back of the reflective surface, which decays within a third of the wavelength.

On the other side of the sensor chip, the protein or ligand can be immobilized on the surface through covalent bonding or other types of bonding. A buffer is used in between to rinse off the unbound form and then the ligand or protein is flowed through the surface. The wavelength of incident light is around 500 nm so that the evanescent waves could extend for at least 100 nm from the back of the reflective surface. When the protein or ligand binds to the species that is coupled on the surface, the increased mass will affect the sensitive evanescent light wave and change the refractive index and ultimately generate signal.

Here we mainly use SPR to study the interaction of Aβ peptide with Brichos protein by immobilizing Aβ monomers or fibrils onto the surface of the gold chip and passing the Brichos protein to see if there is any interation between these proteins. Mass increase on the surface will be observed if there is any association between them. Quantitative information, i.e. binding affinity, the on and off rate constants can be calculated by fitting rate equations to the binding curves.

Mass spectrometry and crosslinking

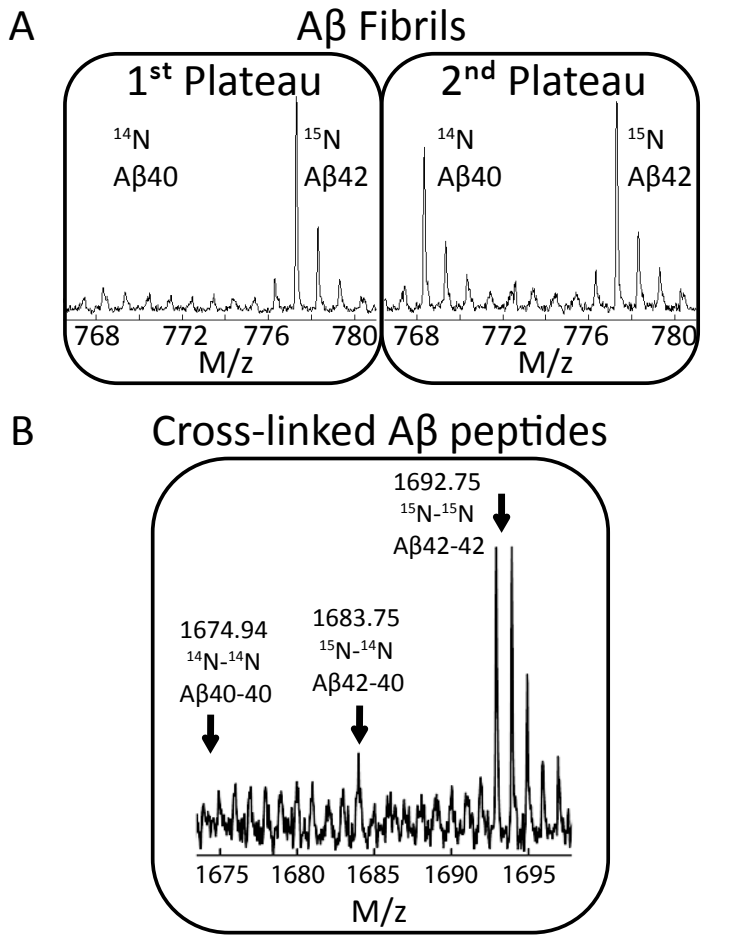

Figure 10: Mass spectra of Aβ fibrils and crosslinked Aβ peptides. Aβ40 peptide is isotope labeled with ^{15}N to be differentiated from Aβ42 after trypsin digestion. Signals shown in the spectra are from peptide segment AβM1-5. A) MS measurement on Aβ fibrils that are formed at the first and second plateau. B) Dimers captured at the lag phase by crosslinking. The spectrum is a sum of 7 measurements from the same sample spot.

Mass spectrometry (MS) is a technique to detect the molecular mass of sample. Simply, the instrument shoots the sample with a laser, and the molecules in the sample becomes ionized because of the interaction with high speed electrons. The ions are accelerated in an electric or magnetic field and separated according to their mass-to-charge ratio (m/z). The ions can be detected in several ways, among which

the most frequently used one is called time of flight (TOF). TOF detectors is to measure the time it takes for a molecule to fly over a certain distance, which is proportional to m/z. The result is shown as a mass spectrum, a plot of the ion peaks as a function of the m/z. The molecules can be identified directly by the mass or through a characteristic fragmentation pattern.

To make biological macromolecules such as proteins ionized better, a method called matrix-assisted laser desorption ionization (MALDI) is usually used. The protein is mixed with a matrix, which usually contains organic micro-crystalline, and applied on the sample plate to be air dried. When the laser shoots the sample spot, the matrix absorbs energy and becomes ionized and later transfers protons to the protein. Therefore, the protein gains charge through this event and the chance of ionization is increased.

Besides molecular identification, MS can be used to study the structure or protein-protein interaction by crosslinking the samples with a linker with designed arm length. BS3 is a commonly used crosslinker with 12 Å arm length and it links the primary amines on the peptide chain. Usually coupled with crosslinking, trypsin digestion is used to generate ionizable small protein fragments. Aβ40 is expressed with ^{15}N so as to show a different mass from Aβ42 after trypsin digestion. Detection of the crosslinked protein segments suggests the possible interaction between these species. By analyzing signals of the crosslinked sequences, the protein structure can be deducted by comparing with the possible linkages.

Kinetic analysis

After the aggregation kinetic data is acquired, there are several steps for the analysis. Firstly, we define the aggregation half-time as the time point when half of the peptide population has formed aggregate. ThT fluorescence reaches half way of the maximum increase and the correspondent half-time is shown as and example in Fig. 7. The half-time can be extracted by fitting the experimental data with an empirical sigmoidal equation (Eq. 5) that is described in below,

$$F(t) = F_0 + \frac{F_{\max} - F_0}{1 + e^{-k(t - t_{1/2})}} \tag{5}$$

The fitting parameters are shown as, F_{max}, the amplitude of fluorescence intensity increase, F_0, the baseline intensity, $t_{1/2}$, the aggregation half-time, and k, an apparent elongation rate constant. To go one step further, the half-time extracted from a concentration-dependent kinetic experiment can be plotted versus the peptide con-

centration. This data is then fitted by a power function (Eq. 6) to obtain a scaling exponent γ,

$$t_{1/2} = Bm_0^{\gamma} \tag{6}$$

In this equation, B is the proportionality constant and m_0 is the initial monomer concentration. The scaling exponent γ reflects the dependency of aggregation half-time on the monomer concentration, and becomes the slope in a log-log plot.

As is mentioned above, from the half-time analysis we can get a scaling exponent that reflects the overall aggregation rate and monomer dependency. Protein aggregation is in general a complicated process that is composed of different microscopic reactions. An aggregation model that is firstly proposed by Knowles' group[47] with an analytical expression solved used in our analysis. In this model, aggregation is described as being composed of several microscopic steps, such as primary nucleation, secondary nucleation, elongation and fragmentation, and a rate constants, k_n, k_2, k_+ and k_- is established for each of them, respectively.

A global fitting tool,[77] a platform that is establish based on Knowles' model, is used to fit the experimental data and extract the individual or combined rate constant of each microscopic reaction. The mechanistic shift of the aggregation behavior that is affected by different factors could then be elucidated in the detailed microscopic reactions by the variation of the rate constants of these microscopic aggregation steps.

Results and discussion

The aim of my PhD work is to study the aggregation mechanism of Aβ in different scenarios. The following papers are discussed individually and the studies are focused mainly on the aggregation mechanistic change as a result of

Intrinsic factors :

Familial mutations that are related to early-onset AD (Paper I and VI).
Peptide length that differs at the C-terminus: Aβ42 and Aβ40 (Paper II and IV).

Extrinsic factors :

Increased ionic strength (Paper V).
A pH shifted close to the isoelectric point of Aβ (Paper IV)
Interation with a chaperone protein (Paper III).

The kinetic experiments are always started with gel filtration to remove aggregates that are formed during freezing and lyophilizing steps. Freshly collected monomer is stored on ice until loaded in the micro-plate for fluorescence reading. ThT is used in a concentration range where the signal is linear with the fibril mass. Data analysis is performed as discribed in the previous chapter. The result shows that these factors mainly affecting the aggregation mechanism in a way of reducing electrostatic repulsion, effect caused by side chain property, obstructing peptide co-aggregate or interacting with a specific species in the aggregation process. Therefore, these intrinsic and extrinsic factors help us to understand Aβ aggregation in microscopic detail and also elucidate the Aβ aggregations in different scenarios.

Paper I

In this paper, we studied the aggregation kinetics of five familial mutants that are mutated in Aβ 21-23 region of the gene, named Flemish (A21G), Iowa (D23N), Dutch (E22Q), Arctic (E22G) and Italian (E22K). The aggregation kinetics was performed as concentration-dependent manner and the stock solution was prepared at 10 μM and diluted to 12 different concentrations down to 0.8 μM with a ThT concentration of 6 μM. The ThT fluorescence increase was recorded as a function of time. The aggregation half-time, as the fluorescent intensity reached the half way, was plotted against peptide concentration using logarithmic axes. By fitting the curves with a power function (Eq. 6). The scaling exponent γ was extracted. The result shows that five mutants except for A21G are more aggregation prone than the wild type and appear at a lower position in the log-log plot. The value of γ increases from -1.8 to -0.6 (Fig. 11). The increase in γ reflects the aggregation is becoming less dependent on monomer concentration, which implies a mechanistic shift in the aggregation process. *Cryo*-TEM image shows that mutant E22Q, E22G, and D23N fibrils are more similar to the Aβ42 wt in that the twisted fibrils have a small node-to-node distance, short length and close interaction between fibrils. A21G shows longer fibrils and a longer node-to-node distance. E22K also shows longer fibril length but with more bundles that are composed of several fibrils.

By fitting the large body of aggregation data of all five mutants with different models that employ several master equations derived from the previous publication[47] on the global fitting platform Amylofit,[77] a multi-step secondary nucleation dominant aggregation mechanism is revealed for all the charge mutants. The aggregation of A21G is dominated by secondary nucleation, as Aβ42 wt reported before.[49] For the charge mutations, both the primary and secondary nucleation are significantly enhanced and the latter one becomes saturated at the higher concentration or even in the full concentration range tested for some of the mutants. By saturation, it means that the rate of the secondary nucleation that is catalyzed by the surface of the fibril is relying on the rate limiting dissociation of nuclei from the surface rather than the monomers association on the surface. This yields an aggregation mechanism shift from a monomer-dependent way to a monomer independent manner, thus, lead to an increased γ. The enhancement of secondary nucleation in the mutant aggregation is confirmed with seeding experiments which show drastic decrease on half-time after adding fibrils to the monomer solution and is seed-concentration-dependent.

The main reason for this mechanistic shift is very likely due to a reduction of absolute charge for all mutants except for A21G. That explains why A21G has an aggregation behaviour more like Aβ42 wt with a close value of both primary nucleation and

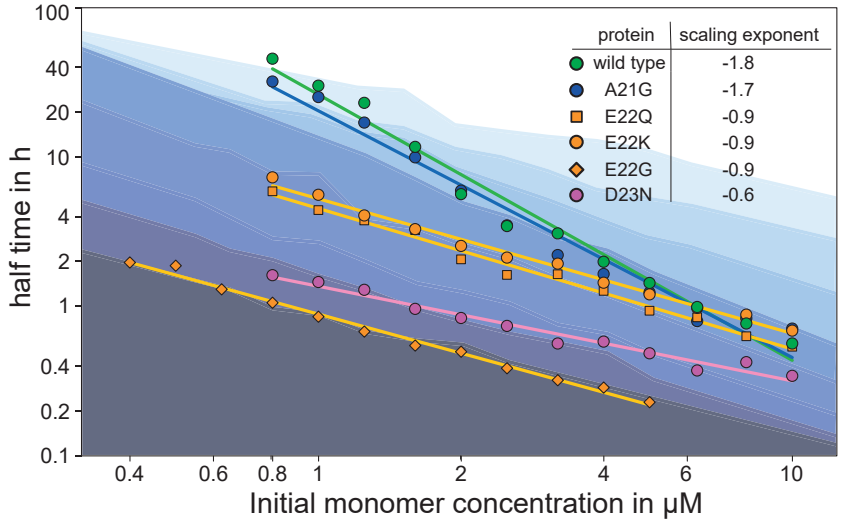

Figure 11: Aggregation half-time of all five familial mutants and Aβ42 wt plotted against initial monomer concentration in logarithmic scale. The shading in the background represents aggregation half-time at different ionic strengths ranging from 12 mM (lightest) to 312 mM (darkest).

secondary nucleation rate constants. The role it plays in the disease is more likely linked to its overexpression and higher resistance against protein digestion compared to other variants.[30,31] Other mutations in site E22, E22K, E22Q and E22K, show a similar scaling exponent around -0.9. implying a similarity of mechanism shift to a less concentration-dependent process and the saturated secondary nucleation. D23N shows the flattest scaling, -0.6, which is the least concentration-dependent and highly saturated secondary nucleation. The weakened electrostatic repulsion due to reduced charge on all these four mutants takes the main responsibility of the aggregation propensity change. At pH 8.0, Aβ42 wt has a net charge around -3, the long-range electrostatic repulsion is largely decreased from these mutants with 1 to 2 charge reduction. This lead to a lower boundary for the primary and secondary nucleation shows faster aggregation half-time. Additional factors play a role in mutant D23N and E22G, for which the aggregation is severely enhanced, and E22K, for which the more charge reduction but not as significant increase in aggregation half-time. These effects might be attributed to the side chain property, such as size, steric hindrance and hydrophobicity.

Paper II

Protein aggregation in a mixed system is of great interest due to the co-localization of different variants. The most abundant Aβ variants found *in vivo* are Aβ40 and Aβ42. The latter one has two additional amino acid isoleucine and alanine at C-terminus. Due to the more hydrophobic C-terminus, Aβ42 is more aggregation prone compared to Aβ40, yielding a much shorter half-time. At equivalent concentration, Aβ42 shows a much lower ThT fluorescence and a similar sigmoidal aggregation curve compared to Aβ40. To my knowledge, double sigmoidal in aggregation of the Aβ40 and Aβ42 mixture was observed here for the first time.

We started with mixing the Aβ42 and Aβ40 peptides in 1:1 ratio with a total concentration ranging from 1 to 10 μM. Interestingly, not like pure Aβ42 or Aβ40 alone, instead of having one sigmoidal aggregation curve, there are two sigmoidal transitions with the latter one following after the first. According to the half-time and fluorescence intensity difference between the two Aβ variants, we speculate the first sigmoidal transition corresponds to the aggregation of Aβ42 in the mixture while the second sigmoidal is more likely due to the aggregation of Aβ40. Fibrils taken from each plateau were imaged using *cryo*-TEM and compared with the fibrils formed in the pure forms. When they aggregate separately, the Aβ42 and Aβ40 fibril morphologies show distinct differences in length, thickness, and node-to-node distance. The images show that fibrils taken from the first plateau are more like Aβ42 fibrils and a mixture of both forms of fibrils are seen at the second plateau. Node-to-node measurement demonstrates this speculation in a more quantitative way. Moreover, we performed MS to see the depletion of monomers in the solution and the components in the fibrils, by taking out solutions during the aggregation process at different time points, centrifuging samples to separate the supernatant and fibrils. The MS result shows the ratio of Aβ42:Aβ40 is 1:1 at t_0 and gradually decreases to close to 0 at the end of the first transition (Fig. 12). While there is hardly any Aβ42 left after the first plateau, Aβ40 is still presenting until reaching the second plateau. MS analysis for the fibrils that were collected at the first and the second plateau also shows that the first plateau is with mostly Aβ42 fibrils and the second plateau contains both Aβ42 and Aβ42 fibrils, which is in line with our finding using TEM. Monomer depletion measurement by NMR shows a consistent result that Aβ42 depletes first and then Aβ40.

So far we conclude that these two variants can not co-aggregate and form mixed fibrils. But compared with the pure Aβ peptide aggregation, still there is an acceleration noticed for the second plateau. To investigate at which step and to what extent these two variants interfere with each other in the aggregation process, we performed self-seeding and cross-seeding experiments.

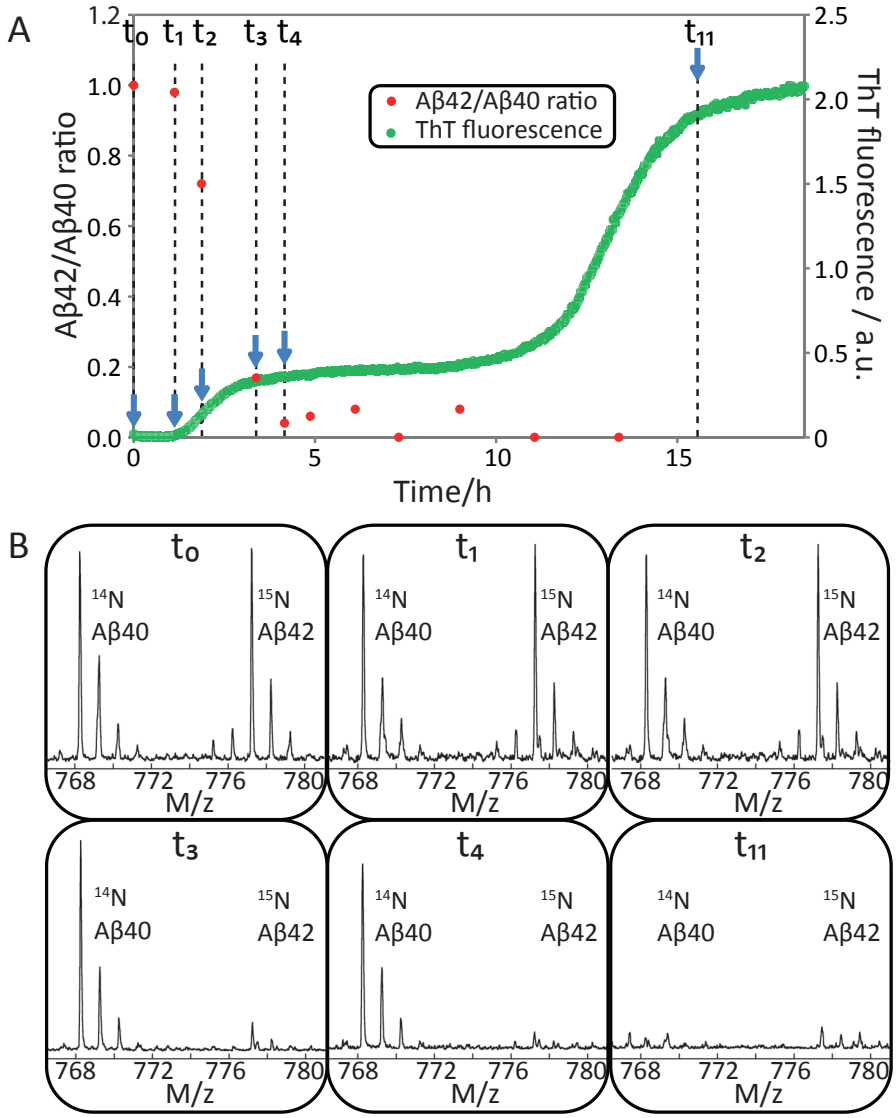

Figure 12: Aggregation of a mixture of 1.5 µL Aβ42 and 1.5 µL Aβ40 that is followed by ThT fluorescence and mass spectrometry. Aβ42/Aβ40 ratio decreases close to 0 after the first plateau is reached.

As reported in previous studies, the aggregation mechanism for both variants is dominated by secondary nucleation, which serves as a feedback loop reaction and accelerates the whole process.[49] The self-seeding was efficient for both variants. On the contrary, the cross-seeding seems to have no accelerating effect at all.

Even adding seed to the mixture of Aβ40 and Aβ42 was only selectively accelerating the same species as in the seed. Therefore, we can rule out that the two variants interact during secondary nucleation or elongation. What is left among the possible microscopic steps is the primary nucleation. To test if they interact at the primary nucleation level, aggregation was followed at constant concentration of one variant and increasing concentration of the other one. The results show that an increase in monomeric Aβ40 is not affecting the aggregation of Aβ42. On the other hand, an increase in Aβ42 accelerates the aggregation of Aβ40. Data fitting shows that the aggregation of Aβ40 is not affected in the secondary process but only with a shorter lag phase which implies accelerated primary nucleation. The only possibility is then interaction with Aβ42 monomers, and form co-nuclei that somehow accelerates the primary nucleation of Aβ40 peptides. But later on the peptides aggregate separately though a more efficient secondary nucleation pathway. The reason lying behind the kinetics is very likely due to a more involved C-terminus in the core region of the fibrils that is reported in several structure models[67] and this tolerates a low-level miss match of sequence homogeneity, in our case, at the C-terminus. While primary nucleation leads to formation of smaller and less organized structures, it might accommodate the small difference in the C-terminus.

Paper III

Aβ42 aggregation mechanism has earlier been reported, which is dominated by secondary nucleation that is providing a catalytic cycle and boosting oligomer production. A chaperone protein, Brichos, was previously reported to inhibit protein misfolding including Aβ42 aggregation.[78] In this paper, a particular microscopic process of Aβ42 aggregation, secondary nucleation, is found to be targeted by Brichos, which leads to a significant decrease of toxic oligomer production.

Kinetic tests combined with global fitting shows that Brichos mainly inhibits secondary nucleation, which dramatically reduces the total oligomer production by 84%. On the contrary, inhibiting primary nucleation only delays the oligomer production but does not change the population. Inhibition of elongation will increase the oligomer production by 400% by redirecting the aggregation process to secondary nucleation. To investigate which species Brichos interacts with, a kinetics experiment was set up with monomeric Aβ42 added with fibrils formed with Brichos present or absent and monomeric Aβ42 with Brichos added with fibril formed with Brichos present of absent. The results show that Aβ42 aggregation is accelerated by fibrils treated with Brichos to a less extent (roughly 40%) than fibrils formed without Brichos, meaning most of the chaperone proteins stayed on the surface and inhibited the secondary nucleation. When Aβ42 monomer and Brichos mixture was supplemented with fibrils formed with Brichos present or absent, all curve indicative of inhibited secondary nucleation, which means that Brichos can inhibit ongoing aggregation reactions. To further investigate the molecular interaction between Brichos and various Aβ species during aggregation, negative stain TEM was applied on the fibril sample with gold nanoparticles conjugated with anti-Brichos antibody. Images show that gold particles bind along the fibrils suggesting that Brichos proteins are mainly located on the fibril surface. Meanwhile, binding of Brichos to Aβ fibril or monomer was studied by injecting Brichos and flowing over a surface that is conjugated with Aβ42 fibril or monomer. The result shows binding on the fibril-coated surface but not on the monomer covered surface or the control channel, which further supports the specific interaction with Aβ42 fibrils.

Low molecular weight Aβ42 assemblies were quantified by fractionating seeded Aβ42 solution and using an Aβ42 sensitive antibody for detection. Smaller (14-65 kDa) and larger oligomers (66-90 kDa) were detected in the seeded sample without Brichos present. On contrary, the seeded Aβ42 sample with Brichos present shows a substantial decrease in oligomer production, which is consistent with the prediction made in this work. *Cryo*-TEM shows that fibrils formed in the presence of Brichos are overall longer than without Brichos (Fig. 13). It is another proof of the redirection of secondary nucleation to elongation. Furthermore, an electrophysiology

method was used to test if the suppression of oligomer production also decreases the neurotoxicity. The mouse brain slices were treated with Aβ42 peptides with Brichos presence or absence. In this method, hippocampal γ oscillation was detected, and a reduced signal suggests brain damage and is related to neurodegenerative disease syndrome. The results show that the seeded Aβ has the highest toxicity, and the effect can be rescued in the presence of Brichos.

In conclusion, the secondary nucleation is effectively inhibited, and oligomeric Aβ42 and its toxicity are significantly suppressed when Brichos is introduced into the system. Brichos proteins specifically interact with Aβ42 fibrils and block the catalytic surface, which is the cause behind the inhibition. This result may help to develop a treatment of in an early stage by introducing a secondary nucleation inhibitor to suppress the production of toxic oligomeric Aβ species so as to reduce the neurotoxicity.

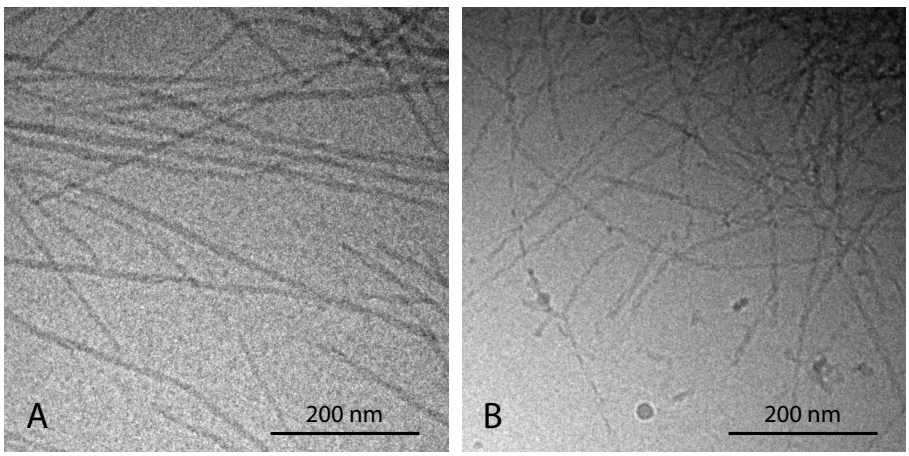

Figure 13: *Cryo*-TEM images of Aβ fibril. Scale bar = 200 nm. A) Aβ42 fibrils formed in the presence of Brichos. B) Fibrils formed only by Aβ42.

Paper IV

In this paper, we have studied the aggregation mechanism of Aβ40 and made a comparison with Aβ42 aggregation according to individual microscopic aggregation steps.

Highly reproducible kinetic data of Aβ42 aggregation were performed using recombinant peptide and aggregation was followed by using ThT assay at a concentration range of 3.5-70 μM. The half-time was extracted as the time point where half amount of the peptides was folded into the aggregate form. A power function (Eq. 6) was used to fit the half-time versus concentration, and a scaling exponent γ was obtained, which gives the implication of the dominant microscopic steps in the aggregation mechanism. Interestingly, a concentration-dependent scaling exponent was found both at lower concentration (below 5 μM) $\gamma = -1.2 \pm 0.2$ and at higher concentration (above 60 μM), where γ became -0.2 ± 0.05. The scaling exponent variation suggests a change in microscopic processes and leads to a different monomer dependence in different concentration ranges. This change is very likely due to secondary nucleation rather than elongation.

Models developed in the previous studies[47,49,79,80] were used to study the Aβ40 aggregation mechanism on a detailed microscopic level. The saturation of secondary nucleation can be described using Michaelis-Menten-like kinetics and Langmuir-like adsorption as an analogy. By introducing the saturation into the fitting model, the half-time versus concentration could be globally fitted, whereas poor fit to the data set was obtained if the model contains single step secondary nucleation, only fragmentation or these two secondary pathways in parallel. The half-time at each concentration was predicted by using the rate constants aquired from global fitting. The predicted half-time agrees well with the actual data at concentrations below 30 μM. At higher concentration, the minimal slope calculated from the rate law is -0.5, which differs from the experimental value -0.2. The even less monomer dependent aggregation at the higher concentration range is later shown to be due to saturated elongation. By performing seeding experiments, the initial gradient that is due to elongation is increasing as the initial monomer concentration increases in a linear manner when the monomer concentration is below 30 μM. The increase of initial gradient is not as prominent at a monomeric concentration higher than 30 μM, which suggests a saturation of elongation.

The saturation model developed in the current paper can be used to describe the aggregation mechanism of Aβ40 at concentrations lower than 30 μM. The rate constants achieved from the fitting are then used to compare with Aβ42. To get the individual rate constant k_+, k_n and k_2 instead of rate constants combinations

k_+k_2 and k_+k_n, k_+ is estimated by defining the average fibril length according to the TEM images and application of the master equations to data for seeded samples. Results show that all rate constants of Aβ40 are lower than Aβ42 (Fig. 14). Moreover, primary nucleation shows the most severe decrease among all three rate constants, which reflects that secondary nucleation plays a more important role in the Aβ40 fibril production. The more drastic decline of primary nucleation rate than the other two constants implies that the additional hydrophobic amino acids, isoleucine and alanine, in Aβ42 lower the energy barrier of aggregation.

In conclusion, aggregation mechanism of Aβ40 is revealed that dominated by secondary nucleation, like Aβ42, but shows a saturated secondary nucleation and elongation at a concentration higher than 30 μM. Individual rate constants k_+, k_n and k_2 of Aβ40 are all lower than that of Aβ42 with a particular reduction in the kn, which suggests that the additional two amino acids of Aβ42 at the C-terminus lower the energy barrier during the aggregation and the barrier effect is more significant in primary nucleation than the monomer association and nuclei formation on the fibril surface. While the kinetics test for Aβ42 was performed at pH 8.0, Aβ40 aggregation was tested at pH 7.4 due to a faster aggregation and better data reproducibility at low concentration, which means an even larger difference of the rate constants between Aβ40 and Aβ42 would be obtained at the same physiological pH.

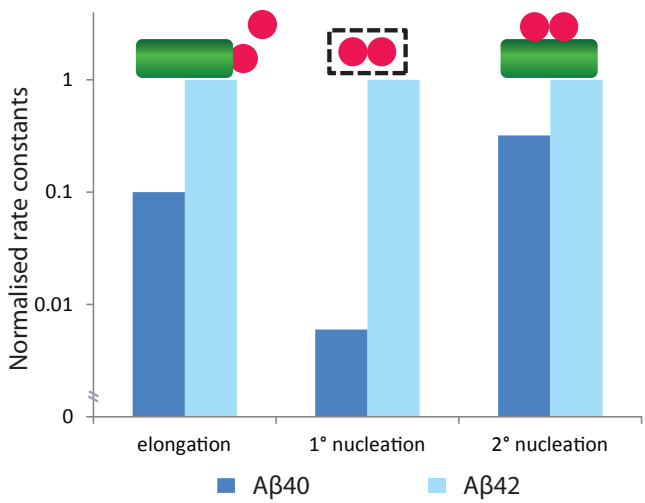

Figure 14: Comparison of elongation rate, primary nucleation rate and secondary nucleation rate between Aβ42 and Aβ40.

Paper V

In this paper, the aggregation mechanism of Aβ42 has been studied in a concentration-dependent manner at ionic strengths ranging from 12 mM to 312 mM. A model is developed here to fit the whole set of data and provide quantitative explanations to the aggregation behaviour at low and high ionic strengths and uncover the aggregation mechanism shift due to the electrostatic shielding by adding salt.

Firstly, Aβ42 aggregation kinetics was performed in a concentration-dependent manner from 0.55 to 7 μM, in 4 mM phosphate buffer at pH 8.0 with additional NaCl of a final concentration from 0 to 300 mM. The half-time was then extracted and plotted in a log-log manner for each salt concentration. The decrease in half-time upon increase in ionic strength was observed and such effect is due to the screening of electrostatic repulsion between the aggregating species by salt. TEM images show that fibril formed in low ionic strength (29 mM) are more evenly distributed compared to fibrils formed at high ionic strength (329 mM) where there is more lumping (Fig. 15 B and C). To go beyond the overall aggregation rate, a power function was used to fit the half-time versus monomer concentration to extract a scaling exponent γ, which reflects the monomer dependency of the aggregation process. The result shows the scaling exponent decreases from -0.7 at low ionic strength to a minimum value of -1.4 at medium ionic strength (around 32 mM), and then increase to -0.6 at the highest ionic strength (Fig. 15 A). The monomer dependence is greatest when the ionic strength is around 32 mM but less dependent at both low and high ionic strength. Besides, some curves at low ionic strength show different monomer dependence, resulting in a flatter slope (higher γ) at lower concentration and steeper slope (lower γ) at higher concentration. The opposite slope change was observed at higher ionic strengths. To explain the shift of the scaling exponent at low and high ionic strength and the change in monomer dependency, we here propose two particular cases base on the general aggregation model, which includes both fragmentation and secondary nucleation. One case is a parallel model in which both secondary nucleation and fragmentation are crucial. The other is a saturation model where the reaction is dominated by saturated secondary nucleation and fragmentation is negligible. Saturation of elongation is not observed in our case in heavy seeding experiments, and is not considered here.

By fitting the aggregation data with these models, we found that at low ionic strength between 12 mM and 20 mM, fragmentation and secondary nucleation both are important. While fragmentation is dominant at low monomer concentration (γ is between -0.5 and -1.0), secondary nucleation is dominant at higher monomer concentration (γ is around -1.5), resulting in an average scaling exponent of circa -1.0. At ionic strengths between 22 mM to 62 mM, the aggregation is mainly

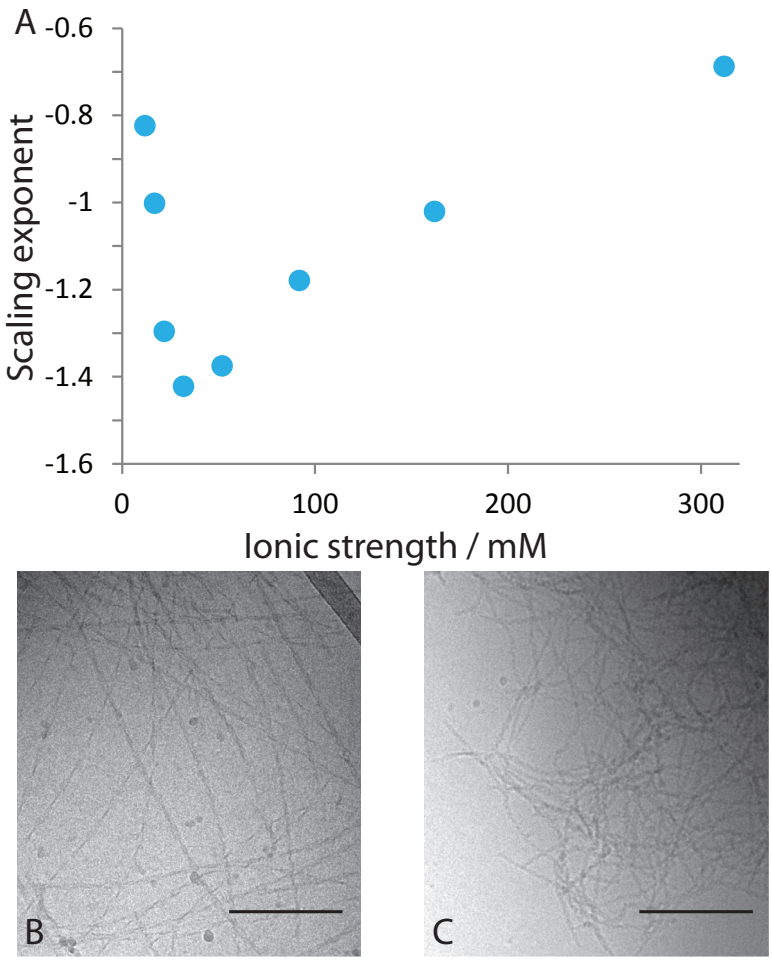

Figure 15: A) The scaling exponent of Aβ42 as a function of ionic strengths. Higher γ at both high and low salt concentration reflecting the mechanistic shift at different ionic strength. B) and C) Aβ42 fibril formed at low ionic strength (29 mM) and high ionic strength (329 mM), respectively. Scale bar = 200 nm.

dominated by secondary nucleation and monomer dependence, which is consistent over the entire concentration range studied with a scaling exponent around -1.4. At ionic higher strength around 92 mM, the secondary nucleation starts to get saturated at higher monomer concentration resulting a scaling shift from -1.4 to -1.0. At ionic strength higher than 162 mM, the secondary nucleation is fully saturated, and the scaling is approaching back to -0.5.

Paper VI

This paper summarizes the experimental approach to generate reproducible data and global kinetic fitting to analyse the aggregation mechanism, which is shifted due to an intrinsic factor, e.g. amino acid substitution or an extrinsic factor, e.g. a pH change.

High quality reproducible kinetic data are the crucial prerequisite for obtaining a reliable kinetic analysis. Here we discussed several key points that matter for the reproducibility. Any minor impurities in the sample will make the system a more complicated case and may redirect the conclusion from the true story. In the latter half of the paper, Aβ aggregation kinetics as a result of intrinsic factor, e.g. point mutation, or extrinsic factor, pH change, are studied and a saturated secondary nucleation is observed for both cases.

We express Aβ peptide as a recombinant form in *E.coli* which produces homogeneous peptide sequence as a result of the high fidelity of the protein translation machinary. The peptide is expressed without a tag to high yield and forms inclusion bodies, which are simply purified by sonication and washing with buffer. After dissolving the inclusion bodies in urea, the peptide is purified by IEC in batch mode to avoid high local concentration on the resin and then followed by one or two rounds of SEC purification. From the previous findings, a trace amount of aggregates will serve as a catalyser and change the aggregation rate. Thus, a second round of SEC filtration is essential for setting up the kinetic experiment. Secondly, since Aβ peptide is surface active, the labware used to handle the sample need to be of low-binding material with a well-controlled air-water interface to avoid perturbation of the aggregation system. Co-solvents and buffer conditions are important in a way that the former may alter the aggregation of Aβ and the latter one changes the dominant microscopic aggregation steps with a different pH, temperature or ionic strength. Thirdly, the method that is chosen to follow the kinetic process needs to be stringently confirmed in terms of the signal that reflects the actual value of the target. The data are acquired at quiescent conditions to avoid promoting the fragmentation. At last, the constraints that are needed for the fitting need to be considered in the experimental design.

Within this framework, the aggregation kinetics of Aβ42 with a point mutation A2V and pH change from 8.0 to 7.4 was studied and a mechanistic shift to saturated secondary nucleation dominant aggregation is found for both of the cases. More specifically, the combined rate constants of k_+k_n and k_+k_2 have increased for one to two orders of magnitude (Fig. 16). The increased aggregation is probably due to an increase in hydrophobicity for A2V and a reduced electrostatic repulsion as pH

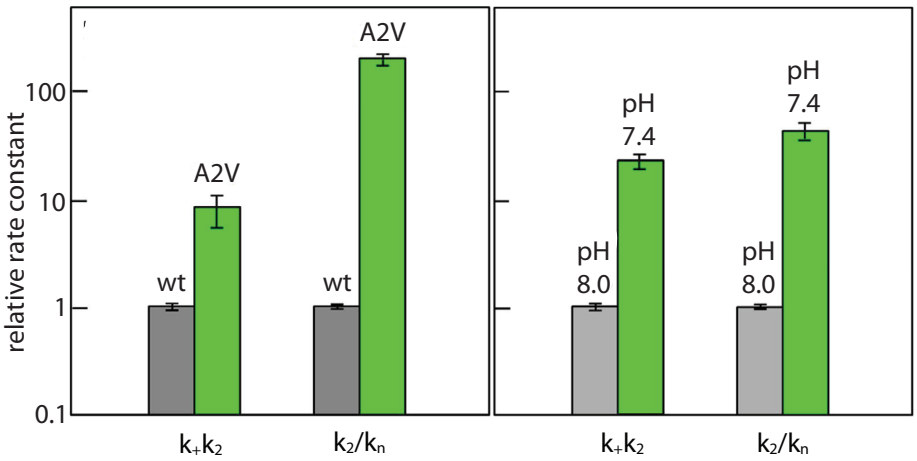

Figure 16: Comparison of combined rate constants k_+k_n and k_+k_2 for intrinsic changes (Aβ42 wt and A2V) and extrinsic changes (pH 8.0 and pH 7.4)

shifts to 7.4, which suggests the binding affinity of monomers to the fibril surface is promoted by the two factors and the same mechanistic change can be originated from different factors.

Concluding Remark

Our work shows a well-established approach to study Aβ aggregation kinetics. The expression of recombinant Aβ in *E.coli* plus the purification by performing batch mode IEC and multiple runs of SEC guarantee the high purity, sequence homogeneity and high yield of protein production. Therefore, the experimental kinetic data are achieved in high reproducibility, which is essential for data fitting so as to get a more accurate estimation on the rate constant of each microscopic reaction. The global fitting to the experimental data using a master equation approach reproduces the aggregation kinetics fairly well. By doing this we are able to obtain the individual rate constants or rate constants in combination, which helps us to value the importance of each microscopic step and unravel the kinetic mechanism shift.

The dominant aggregation process that is shifted to a secondary nucleation is the main finding in most of the scenarios we have tested. The mechanistic shift is mostly attributed to the decrease in electrostatic effect when introducing charge mutations (E22Q, E22K, E22G, D23N), increasing the salt concentration, or moving pH to a value that is close to the isoelectric point. These approaches lead to either a weakened electrostatic repulsion by bringing down the absolute net charge (point mutation or lowering pH), or screen the Debye length (adding salt).

However, for some point mutation, the electrostatic effect is not able to fully explain the severely enhanced aggregation propensity, e.g. E22G, D23N, a boost in secondary nucleation that is not proportionally to the reduced charge (E22K), and not at all elucidated the non-charged mutation A2V. In this case, the inserted amino acid side chain property, e.g. size, steric hindrance and hydrophobicity is the likelihood of driving the mechanism shift to the enhanced secondary nucleation. The hydrophobic effect also contribute in Aβ42 aggregation due to the additional two amino acid at the C-terminus.

Co-aggregation of Aβ40 and Aβ42 shows that the mismatch in the C-terminus hinders the peptides to co-aggregate and form a highly ordered structure. This may be related to the structure of a berried C-terminus in the fibril core in structure

models that aquired in several NMR studies.[67]

The chaperone protein Brichos that previously found to retard Aβ aggregation here reveals that due to the specific interation with the fibril surface, it is able to lower or completely halt the secondary nucleation, thus, break the catalytic cycle that produces enormous amount of oligomers.

Overall, we have shown that the relative reaction rates and importance of the different microscopic steps underlying the amyloid beta aggregation is affected by several intrinsic and extrinsic factors leading to a similar mechanistic shift. Our findings are of high relevance as the secondary nucleation step lies behind the generation of the vast majority of toxic species. The results also imply that the microscopic reactions are tunable by different approaches, which may provide information for targeting a specific aggegation event and may be useful in the development of the therapies for AD.

References

[1] K Blennow, M J de Leon, and H Zetterberg. Alzheimer's disease. *Lancet*, 368(9533):387–403, 2006.

[2] Yat-Fung Shea, Leung-Wing Chu, Angel On-Kei Chan, Joyce Ha, Yan Li, and You-Qiang Song. A systematic review of familial Alzheimer's disease: Differences in presentation of clinical features among three mutated genes and potential ethnic differences. *Journal of the Formosan Medical Association*, 115(2):67–75, 2015.

[3] Martin Prince, Anders Wimo, Maëlenn Guerchet, Ali Gemma-Claire, Yu-Tzu Wu, and Matthew Prina. World Alzheimer Report 2015: The Global Impact of Dementia - An analysis of prevalence, incidence, cost and trends. *Alzheimer's Disease International*, page 84, 2015.

[4] Russell H. Swerdlow. Pathogenesis of Alzheimer's disease. *Clinical interventions in aging*, 2(3):347–359, 2007.

[5] Russell H. Swerdlow. Alzheimer's disease pathologic cascades: Who comes first, what drives what. *Neurotoxicity Research*, 22(3):182–194, 2012.

[6] J. A. Hardy & G. A. Higgins. Alzheimer's Disease: The Amyloid Cascade Hypothesis, 1992.

[7] Eanes ED Glenner GG, Wong CW, Quaranta V. The amyloid deposits in Alzheimer's disease: their nature and pathogenesis. *Appl Pathol*, 2(6):357–69, 1984.

[8] Dennis J Selkoe. Alzheimer ' s Disease : Genes , Proteins , and Therapy. *Perspective*, 81(2):741–767, 2001.

[9] D Scheuner, C Eckman, M Jensen, X Song, M Citron, N Suzuki, T D Bird, J Hardy, M Hutton, W Kukull, E Larson, E Levy-Lahad, M Viitanen, E Peskind, P Poorkaj, G Schellenberg, R Tanzi, W Wasco, L Lannfelt, D Selkoe, and S Younkin. Secreted amyloid beta-protein similar to that in the senile plaques of Alzheimer's disease is increased in vivo by the presenilin 1 and 2 and APP mutations linked to familial Alzheimer's disease. *Nature medicine*, 2(8):864–870, 1996.

[10] Hansa Basun, Nenad Bogdanovic, Martin Ingelsson, Ove Almkvist, Jan Naslund, Karin Axelman, Thomas D. Bird, David Nochlin, Gerard D. Schellenberg, Lars-Olof Wahlund, and Lars Lannfelt. Clinical and Neuropathological Features of the Arctic APP Gene Mutation Causing Early-Onset Alzheimer Disease. *Arch Neurol*, 65(4):499–505, 2008.

[11] Hui Zheng and Edward Koo. Biology and pathophysiology of the amyloid precursor protein. *Molecular Neurodegeneration*, 6(1):27, 2011.

[12] MA Pericak-Vance EH Corder, AM Saunders, WJ Strittmatter, DE Schmechel, PC Gaskell, GW Small, AD Roses, JL Haines. Families, Gene dose of apolipoprotein E type 4 allele and the risk of Alzheimer's disease in late onset. *Science*, 261(5123):921–923, 1993.

[13] Min Xu, Ming-Tain Lai, Qian Huang, Jillian DiMuzio-Mower, José L Castro, Timothy Harrison, Alan Nadin, Joseph G Neduvelil, Mark S Shearman, Jules a Shafer, Stephen J Gardell, and Yue-Ming Li. gamma-Secretase: characterization and implication for Alzheimer disease therapy. *Neurobiology of aging*, 23(6):1023–30, 2002.

[14] Dennis Selkoe and Raphael Kopan. NOTCH AND PRESENILIN: Regulated Intramembrane Proteolysis Links Development and Degeneration. *Annual Review of Neuroscience*, 26(1):565–597, 2003.

[15] W P Esler and M S Wolfe. A portrait of Alzheimer secretases–new features and familiar faces. *Science (New York, N.Y.)*, 293(5534):1449–54, 2001.

[16] Christian Haass, Michael Schlossmacher, Albert Hung, Carmen Vigo-Pelfrey, Angela Mellon, Beth Ostaszewski, Ivan Lieberburg, Edward Koo, Dale Schenk, David Teplow, and Dennis Selkoe. Amyloid β-Peptide is Produced by Cultured Cells During Normal Metabolism. *Nature*, 356:133–135, 1992.

[17] M P Lambert, A K Barlow, B A Chromy, C Edwards, R Freed, M Liosatos, T E Morgan, I Rozovsky, B Trommer, K L Viola, P Wals, C Zhang, C E Finch, G A Krafft, and W L Klein. Diffusible, nonfibrillar ligands derived from Abeta1-42 are potent central nervous system neurotoxins. *Proceedings of the National Academy of Sciences of the United States of America*, 95(11):6448–53, 1998.

[18] Klein AM, Kowall NW, and Ferrante RJ. Neurotoxicity and oxidative damage of beta amyloid 1-42 versus beta amyloid 1-40 in the mouse cerebral cortex. *Ann N Y Acad Sci*, 893:314–20, 1999.

[19] Takeshi Iwatsubo, Asano Odaka, Nobuhiro Suzuki, Hidehiro Mizusawa, Nobuyuki Nukina, and Yasuo Ihara. Visualization of Aβ42(43) and Aβ40 in senile plaques with end-specific Aβmonoclonals: Evidence that an initially deposited species is Aβ42(43). *Neuron*, 13(1):45–53, 1994.

[20] Georg Meisl, Xiaoting Yang, Birgitta Frohm, Tuomas P J Knowles, and Sara Linse. Quantitative analysis of intrinsic and extrinsic factors in the aggregation mechanism of Alzheimer-associated Aβ-peptide. *Scientific reports*, 6(October 2015):18728, 2016.

[21] Robert Tycko. Insights into the amyloid folding problem from solid-state NMR. *Biochemistry*, 42(11):3151–3159, 2003.

[22] Karie N. Dahlgren, Arlene M. Manelli, W. Blaine Stine, Lorinda K. Baker, Grant A. Krafft, and Mary Jo Ladu. Oligomeric and fibrillar species of amyloid-βpeptides differentially affect neuronal viability. *Journal of Biological Chemistry*, 277(35):32046–32053, 2002.

[23] D M Hartley, D M Walsh, C P Ye, T Diehl, S Vasquez, P M Vassilev, D B Teplow, and D J Selkoe. Protofibrillar intermediates of amyloid beta-protein induce acute electrophysiological changes and progressive neurotoxicity in cortical neurons. *The Journal of neuroscience : the official journal of the Society for Neuroscience*, 19(20):8876–8884, 1999.

[24] Dominic M. Walsh and Dennis J. Selkoe. Deciphering the molecular basis of memory failure in Alzheimer's disease. *Neuron*, 44(1):181–193, 2004.

[25] DM Walsh, Igor Klyubin, Julia V Fadeeva, William K Cullen, Roger Anwyl, Michael S Wolfe, Michael J Rowan, and Dennis J Selkoe. Naturally secreted oligomers of amyloid beta protein potently inhibit hippocampal long-term potentiation in vivo. *Nature*, 416(6880):535–539, 2002.

[26] Sascha Weggen and Dirk Beher. Molecular consequences of amyloid precursor protein and presenilin mutations causing autosomal-dominant Alzheimer's disease. *Alzheimer's Research & Therapy*, 4(2):9, 2012.

[27] Feldman RG, Chandler Ka, Levyll LL, and Glaser GH. Familial Alzheimer's disease. *Neurology*, 13:811–24, 1963.

[28] Xiao-chen Bai, Chuangye Yan, Guanghui Yang, Peilong Lu, Linfeng Sun, Rui Zhou, Sjors H W Scheres, and Yigong Shi. An atomic structure of human gamma-secretase. *Nature*, 525:212–7, 2015.

[29] T Gomez-Isla, W B Growdon, M J McNamara, D Nochlin, T D Bird, J C Arango, F Lopera, K S Kosik, P L Lantos, N J Cairns, and B T Hyman. The impact of different presenilin 1 andpresenilin 2 mutations on amyloid deposition, neurofibrillary changes and neuronal loss in the familial Alzheimer's disease brain: evidence for other phenotype- modifying factors. *Brain*, 122(Pt 9):1709–19., 1999.

[30] C Nilsberth, a Westlind-Danielsson, C B Eckman, M M Condron, K Axelman, C Forsell, C Stenh, J Luthman, D B Teplow, S G Younkin, J Näslund, and L Lannfelt. The 'Arctic' APP mutation (E693G) causes Alzheimer's disease by enhanced Abeta protofibril formation. *Nature neuroscience*, 4(9):887–893, 2001.

[31] Vicki Betts, Malcolm A. Leissring, Georgia Dolios, Rong Wang, Dennis J. Selkoe, and Dominic M. Walsh. Aggregation and catabolism of disease-associated intra-Abeta mutations: reduced proteolysis of AβA21G by neprilysin. *Neurobiology of Disease*, 31(3):442–450, 2008.

[32] Brent G Irvine, Omar M El-Agnaf, Ganesh M Shankar, and Dominic M Walsh. Protein aggregation in the brain: the molecular basis for Alzheimer's and Parkingson's diseases. *Molecular Medicine*, 14(7-8):1, 2008.

[33] D M Mann, T Iwatsubo, Y Ihara, N J Cairns, P L Lantos, N Bogdanovic, L Lannfelt, B Winblad, M L Maat-Schieman, and M N Rossor. Predominant deposition of amyloid-beta 42(43) in plaques in cases of Alzheimer's disease and hereditary cerebral hemorrhage associated with mutations in the amyloid precursor protein gene. *The American journal of pathology*, 148(4):1257–1266, 1996.

[34] Claire Shepherd, Heather McCann, and Glenda Margaret Halliday. Variations in the neuropathology of familial Alzheimer's disease. *Acta Neuropathologica*, 118(1):37–52, 2009.

[35] Kristel Sleegers, Nathalie Brouwers, Ilse Gijselinck, Jessie Theuns, Dirk Goossens, Jan Wauters, Jurgen Del-Favero, Marc Cruts, Cornelia M. Van Duijn, and Christine Van Broeckhoven. APP duplication is sufficient to cause early onset Alzheimer's dementia with cerebral amyloid angiopathy. *Brain*, 129(11):2977–2983, 2006.

[36] F Massi and J E Straub. Probing the origins of increased activity of the E22Q "Dutch" mutant Alzheimer's beta-amyloid peptide. *Biophysical journal*, 81(2):697–709, 2001.

[37] William E. Van Nostrand, Jerry P. Melchor, Hyun Soon Cho, Steven M. Greenberg, and G. William Rebeck. Pathogenic Effects of D23N Iowa Mutant Amyloid β-Protein. *Journal of Biological Chemistry*, 276(35):32860–32866, 2001.

[38] J Davis and W E Van Nostrand. Enhanced pathologic properties of Dutch-type mutant amyloid beta-protein. *Proceedings of the National Academy of Sciences of the United States of America*, 93(7):2996–3000, 1996.

[39] Gerwin Roks, F Van Harskamp, I De Koning, Marc Cruts, C De Jonghe, S Kumar-Singh, Aad Tibben, Herve Tanghe, Martinus F Niermeijer, Albert Hofman, J C Van Swieten, C Van Broeckhoven, and C M Van Duijn. Presentation of amyloidosis in carriers of the codon 692 mutation in the amyloid precursor protein gene (APP692). *Brain : a journal of neurology*, 123 (Pt 1:2130–40, 2000.

[40] Brooks WS, Kwok JB, Halliday GM, Godbolt AK, Rossor MN, Creasey H, Jones AO, and Schofield PR. Hemorrhage is uncommon in new Alzheimer family with Flemish amyloid precursor protein mutation. *Neurology*, 63(9):1613–7, 2004.

[41] Levy E, Carman MD, Fernandez-Madrid IJ, Power MD, Lieberburg I, Duinen SG, Bots GT, Luyendijk W, and Frangione B. Mutation of the Alzheimer's disease amyloid gene in hereditary cerebral hemorrhage, Dutch type. *Science*, 248(4559):1124–6, 1990.

[42] Grabowski TJ, Cho HS, Vonsattel JP, Rebeck GW, and Greenberg SM. Novel amyloid precursor protein mutation in an Iowa family with dementia and severe cerebral amyloid angiopathy. *Ann Neurol*, 49(6):697–705, 2001.

[43] Benedetta Bolognesi, Samuel I A Cohen, Pablo Aran Terol, Elin K. Esbjörner, Sofia Giorgetti, Maria F. Mossuto, Antonino Natalello, Ann Christin Brorsson, Tuomas P J Knowles, Christopher M. Dobson, and Leila M. Luheshi. Single point mutations induce a switch in the molecular mechanism of the aggregation of the Alzheimer's disease associated Aβ42 peptide. *ACS Chemical Biology*, 9(2):378–382, 2014.

[44] D M Walsh, I Klyubin, J V Fadeeva, M J Rowan, and D J Selkoe. Amyloid-beta oligomers: their production, toxicity and therapeutic inhibition. *Biochemical Society transactions*, 30(4):552–557, 2002.

[45] Frank A. Ferrone, James Hofrichter, and William A. Eaton. Kinetics of sickle hemoglobin polymerization. II. A double nucleation mechanism. *Journal of Molecular Biology*, 183(4):611–631, 1985.

[46] Sean R. Collins, Adam Douglass, Ronald D. Vale, and Jonathan S. Weissman. Mechanism of prion propagation: Amyloid growth occurs by monomer addition. *PLoS Biology*, 2(10), 2004.

[47] Knowles TPJ, Waudby CA, Devlin GL, Cohen SI, Aguzzi A, M Vendruscolo, Terentjev E, Welland ME, and Dobson CM. An analytical solution to the kinetics of breakable filament assembly. *Science*, 326:1533–37, 2009.

[48] Mookyung Cheon, Iksoo Chang, Sandipan Mohanty, Leila M. Luheshi, Christopher M. Dobson, Michele Vendruscolo, and Giorgio Favrin. Structural reorganisation and potential toxicity of oligomeric species formed during the assembly of amyloid fibrils. *PLoS Computational Biology*, 3(9):1727–1738, 2007.

[49] Samuel I A Cohen, Sara Linse, Leila M Luheshi, Erik Hellstrand, Duncan A White, Luke Rajah, Daniel E Otzen, Michele Vendruscolo, Christopher M Dobson, and Tuomas P J Knowles. Proliferation of amyloid-β42 aggregates occurs through a secondary nucleation mechanism. *Proceedings of the National Academy of Sciences of the United States of America*, 110(24):9758–63, 2013.

[50] Georg Meisl, Xiaoting Yang, Erik Hellstrand, Birgitta Frohm, Julius B Kirkegaard, Samuel I a Cohen, Christopher M Dobson, Sara Linse, and Tuomas P J Knowles. Differences in nucleation behavior underlie the contrasting aggregation kinetics of the Aβ40 and Aβ42 peptides. *Proceedings of the National Academy of Sciences of the United States of America*, 111(26):9384–9, 2014.

[51] Georg Meisl, Xiaoting Yang, Christopher M. Dobson, Sara Linse, and Tuomas P. J. Knowles. A general reaction network unifies the aggregation behaviour of the Aβ42 peptide and its variants. 2016.

[52] O Sumner Makin, Edward Atkins, Pawel Sikorski, Jan Johansson, and Louise C Serpell. Molecular basis for amyloid fibril formation and stability. *Proceedings of the National Academy of Sciences of the United States of America*, 102(2):315–320, 2005.

[53] Mark R Wilson, Justin J Yerbury, and Stephen Poon. Potential roles of abundant extracellular chaperones in the control of amyloid formation and toxicity. *Molecular bioSystems*, 4(1):42–52, 2008.

[54] Louise C Serpell. Alzheimer's amyloid fibrils: structure and assembly. *Biochimica et Biophysica Acta (BBA) - Molecular Basis of Disease*, 1502(1):16–30, 2000.

[55] Astbury WT, Dickinson S, and Bailey K. The X-ray interpretation of denaturation and the structure of the seed globulins. *Biochem J*, 29(10):2351–60, 1935.

[56] M. F. Perutz, B. J. Pope, D. Owen, E. E. Wanker, and E. Scherzinger. Aggregation of proteins with expanded glutamine and alanine repeats of the glutamine-rich and asparagine-rich domains of Sup35 and of the amyloid β-peptide of amyloid plaques. *Proceedings of the National Academy of Sciences of the United States of America*, 99(8):5596–5600, 2002.

[57] M F Perutz, T Johnson, M Suzuki, and J T Finch. Glutamine repeats as polar zippers: their possible role in inherited neurodegenerative diseases. *Proceedings of the National Academy of Sciences of the United States of America*, 91(12):5355–8, 1994.

[58] Horst H. Bauer. Architecture and polymorphism of fibrillar supramolecular assemblies produced by in vitro aggregation of human calcionin. *Journal of Structural Biology*, 115:1–15, 1995.

[59] Abe H and Nakanishi H. Effect of pH on the aggregate formation of a non-amyloid component (1-13). *J Pept Sci*, 9(3):177–86, 2003.

[60] Knowles TP, Smith JF, Craig A, Dobson CM, and Welland ME. Spatial persistence of angular correlations in amyloid fibrils. *Phys Rev Lett*, 96(23):238–301, 2006.

[61] Karolin Klement, Karin Wieligmann, Jessica Meinhardt, Peter Hortschansky, Walter Richter, and Marcus Fändrich. Effect of Different Salt Ions on the Propensity of Aggregation and on the Structure of Alzheimer's Aβ(1-40) Amyloid Fibrils. *Journal of Molecular Biology*, 373(5):1321–1333, 2007.

[62] Harper JD, Lieber CM, and Lansbury PT. Atomic force microscopic imaging of seeded fibril formation and fibril branching by the Alzheimer's disease amyloid-beta protein. *Chem Biol*, 4(12):951–9, 1997.

[63] C S Goldsbury, S Wirtz, S a Müller, S Sunderji, P Wicki, U Aebi, and P Frey. Studies on the in vitro assembly of Aβ1-40: implications for the search for a beta fibril formation inhibitors. *Journal of structural biology*, 130:217–231, 2000.

[64] S B Malinchik, H Inouye, K E Szumowski, and D A Kirschner. Structural analysis of Alzheimer's beta(1-40) amyloid: protofilament assembly of tubular fibrils. *Biophysical journal*, 74(1):537–45, 1998.

[65] Takahiro Watanabe-Nakayama, Kenjiro Ono, Masahiro Itami, Ryoichi Takahashi, David B. Teplow, and Masahito Yamada. High-speed atomic force microscopy reveals structural dynamics of amyloid β_{1–42} aggregates. *Proceedings of the National Academy of Sciences*, page 201524807, 2016.

[66] Jessica Meinhardt, Carsten Sachse, Peter Hortschansky, Nikolaus Grigorieff, and Marcus Fändrich. Aβ(1-40) Fibril Polymorphism Implies Diverse Interaction Patterns in Amyloid Fibrils. *Journal of Molecular Biology*, 386(3):869–877, 2009.

[67] Jun-xia Lu, Wei Qiang, Wai-ming Yau, Charles D Schwieters, Stephen C Meredith, and Robert Tycko. Molecular Structure of β-Amyloid Fibrils in Alzheimer ' s Disease Brain Tissue. *Cell*, 154(6):1257–1268, 2013.

[68] Michael R Sawaya, Shilpa Sambashivan, Rebecca Nelson, Magdalena I Ivanova, Stuart A Sievers, Marcin I Apostol, Michael J Thompson, Melinda Balbirnie, Jed J W Wiltzius, Heather T McFarlane, Anders Ø Madsen, Christian Riekel, and David Eisenberg. Atomic structures of amyloid cross-beta spines reveal varied steric zippers. *Nature*, 447(7143):453–7, 2007.

[69] Jacques-Philippe Colletier, Arthur Laganowsky, Meytal Landau, Minglei Zhao, Angela B Soriaga, Lukasz Goldschmidt, David Flot, Duilio Cascio, Michael R Sawaya, and David Eisenberg. Molecular basis for amyloid-beta polymorphism. *Proceedings of the National Academy of Sciences of the United States of America*, 108:16938–43, 2011.

[70] Thorsten Lührs, Christiane Ritter, Marc Adrian, Dominique Riek-Loher, Bernd Bohrmann, Heinz Döbeli, David Schubert, and Roland Riek. 3D structure of Alzheimer's amyloid-β(1-42) fibrils. *Proceedings of the National Academy of Sciences of the United States of America*, 102(48):17342–17347, 2005.

[71] Aneta T Petkova, Yoshitaka Ishii, John J Balbach, Oleg N Antzutkin, Richard D Leapman, Frank Delaglio, and Robert Tycko. A structural model for Alzheimer ' s beta-amyloid fibrils based on experimental constraints from solid state NMR. *Proceedings of the National Academy of Sciences*, 99(26):16742–7, 2002.

[72] Ivano Bertini, Leonardo Gonnelli, Claudio Luchinat, Jiafei Mao, and Antonella Nesi. A New Structural Model of Aβ40 Fibrils. *J. Am. Chem. Soc.*, pages 16013–16022, 2011.

[73] Takeshi Sato, Pascal Kienlen-Campard, Mahiuddin Ahmed, Wei Liu, Huilin Li, James I Elliott, Saburo Aimoto, Stefan N Constantinescu, Jean-Noel Octave, and Steven O Smith. Inhibitors of amyloid toxicity based on beta-sheet packing of Abeta40 and Abeta42. *Biochemistry*, 45(17):5503–5516, 2006.

[74] Aneta T Petkova, Wai-ming Yau, and Robert Tycko. Experimental Constraints on Quaternary Structure in Alzheimer's beta-Amyloid. *Biochemistry*, 45:498–512, 2006.

[75] Fabrizio Chiti and Christopher M. Dobson. Protein Misfolding, Functional Amyloid, and Human Disease. *Annual Review of Biochemistry*, 75(1):333–366, 2006.

[76] Mahiuddin Ahmed, Judianne Davis, Darryl Aucoin, Takeshi Sato, Shivani Ahuja, Saburo Aimoto, James I Elliott, William E Van Nostrand, and Steven O Smith. Structural conversion of neurotoxic amyloid-β(1-42) oligmers to fibrils. *Nature Structural & Molecular Biology*, 17(5):561–567, 2010.

[77] Georg Meisl, Julius B Kirkegaard, Paolo Arosio, Thomas C T Michaels, Michele Vendruscolo, Christopher M Dobson, Sara Linse, and Tuomas P J Knowles. Molecular mechanisms of protein aggregation from global fitting of kinetic modelsDementia. *Nature Prot.*, 11:252–272, 2016.

[78] Hanna Willander, Jenny Presto, Glareh Askarieh, Henrik Biverstål, Birgitta Frohm, Stefan D. Knight, Jan Johansson, and Sara Linse. BRICHOS domains efficiently delay fibrillation of amyloid β-peptide. *Journal of Biological Chemistry*, 287(37):31608–31617, 2012.

[79] Samuel I A Cohen, Michele Vendruscolo, Christopher M. Dobson, and Tuomas P J Knowles. Nucleated polymerization with secondary pathways. III. Equilibrium behavior and oligomer populations. *Journal of Chemical Physics*, 135(6):1–10, 2011.

[80] Samuel I A Cohen, Michele Vendruscolo, Mark E. Welland, Christopher M. Dobson, Eugene M. Terentjev, and Tuomas P J Knowles. Nucleated polymerization with secondary pathways. I. Time evolution of the principal moments. *Journal of Chemical Physics*, 135(6):1–16, 2011.